Large-Scale Testing of JFE Steel Pipe Crossing Faults: Testing of SPF Wave Feature to Resist Fault Rupture

Final Report

Submitted to:

JFE Engineering Corporation
Yokohama, Japan

By

B. P. Wham

T. D. O'Rourke

H. E. Stewart

T. K. Bond

C. Pariya-Ekkasut

Cornell University
School of Civil and Environmental Engineering
Cornell University
Hollister Hall
Ithaca, NY 14853

December, 2016

TABLE OF CONTENTS

LIST OF FIGURES

LIST OF TABLES

Section 1
Introduction

This report is submitted to the JFE Engineering Corporation (herein referred to as JFE). It presents test results from a program to investigate the performance of 8.5-in. (216-mm)-diameter steel pipe with a JFE wave feature for Steel Pipe Crossing Faults (SPF). The purpose of the testing is to evaluate the ability of the SPF to accommodate axial and bending deformation and assess how the pipe and its specially shaped wave features respond to fault rupture and other types of abrupt soil movement that intersects the pipeline. The work was undertaken in the Cornell Large Scale Lifelines Testing Facility, which is part of the Bovay Laboratory Complex at Cornell University.

1.1. Report Organization

The report is organized into six sections. Section 1 provides introductory remarks. Section 2 presents the results of tensile coupon tests performed on the steel used in JFE pipe. Sections 3 and 4 provide the results of direct axial compression and four-point bending tests, respectively. Section 5 describes the test setup and results of a large-scale split basin fault rupture test. Section 6 summarizes key findings from the preceding sections and provides general conclusions derived from the testing program. Appendix A summarizes additional data from the compression test (Section 3) for large axial displacements as well as strain gage measurement on the wave feature.

1.2. JFE Wave Feature

The technology tested is a geometric inclusion developed by JFE and is referred to in this report as a “wave feature”. All testing was performed on wave features of consistent geometry. A schematic of the wave is presented in Figure 1.1. The wave feature is joined to lengths of straight pipe by circular, full penetration butt welds.

The wave features were manufactured in Japan and shipped to Cornell by JFE. The specimens represent approximate one quarter scale models of a 34 in. (850 mm) diameter pipeline, the smallest typical pipeline diameter for which the wave feature is designed. The pipe and wave feature were constructed of hot rolled steel plate conforming to the JIS SS400 Standard (JIS G3101, 2015). Table 1.1 lists the geometric and material properties of the pipe material as reported in information provided by JFE.

Table 1.1. Geometric and Material Properties of JFE SPF Compression Specimen

Outside Diameter, D	8.5 in. (216 mm)
Wall Thickness, t	0.091 in. (2.3 mm)
Tensile Strength	58 – 74 ksi (400 – 510 MPa)
Yield Strength	44 – 46 ksi (300 – 317 MPa)
Young's Modulus	28.5 – 31.6 x 10^6 ksi (196 – 218 GPa)
Poisson's Ratio	0.27 – 0.29

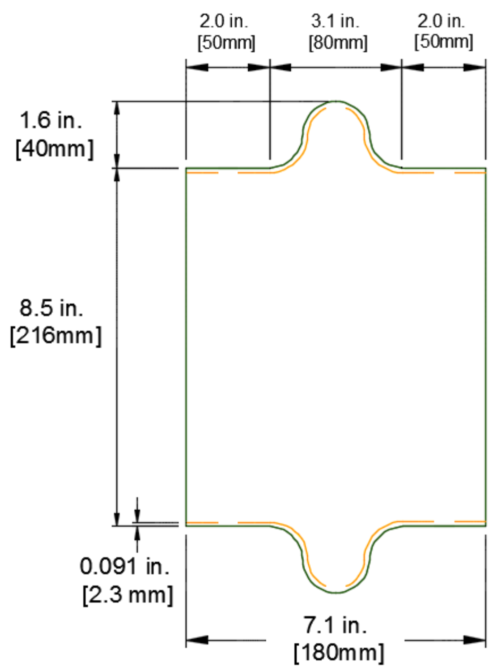

Figure 1.1. SPF Wave Feature Geometry (JFE, Sep. 15, 2015 communication)

JFE provided suggested design values for maximum wave feature deformation. The design values were provided as follows:

- Axial compression: 2.05 in. (52 mm)
- Bending: 18 degrees

These design values were based on numerical analyses performed by JFE and are consistent with deformation values at which contact between internal surfaces of the wave is initiated. Figure 1.2(a) shows highlighted in red a previous test performed by JFE just before reaching internal wave contact. Figure 1.2(b) shows an example of a numerical model at approximately the same deformation level. Multiple waves may be installed in succession to accommodate deformations larger than the design values listed above (e.g., SPF-II, SPF-III). An example of SPF-II is shown in Figure 1.2(a).

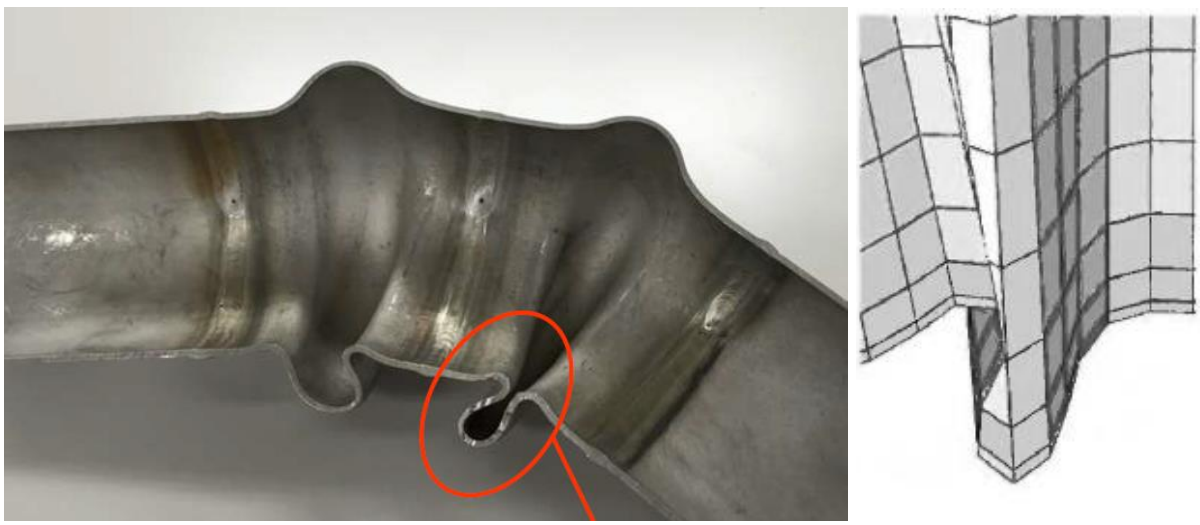

(a) (b)

Figure 1.2. Cross-section of deformed SPF Wave Feature Nearing Design Limit (a) Following Previous Smaller Diameter Testing by JFE and (b) FE analysis

Section 2
Tensile Coupon Tests

2.1. Introduction

This section of the report describes the uniaxial tensile coupon testing and results for hot rolled steel plate specimens provided by JFE. Tensile coupons were machined from a hot rolled steel plate and tested in tension to evaluate the strength, stiffness, and ductility of the material. All testing was conducted in accordance with the ASTM – E8 2013 Standard (ASTM, 2013), and the results are compared to the minimum specifications provided in the JIS SS400 Standard (JIS G3101, 2015).

2.2. Tensile Coupon Testing and Procedure

As provided in ASTM - E8 2013, the nominal dimensions of the tensile coupons are shown in Figure 2.1. The ASTM standard does not identify a specific wall thickness. Each coupon had a nominal thickness, t, of 0.09 in. (2.3 mm). A Baldwin Hamilton 60 BTE Universal Testing Machine was used to apply tensile loads. The load frame was fitted with a pressure sensor to measure force in the system. The machine was calibrated in April of 2015. A photo of the test setup is provided in Figure 2.2.

Three tensile coupon specimens were tested. All three specimens were instrumented with axial and transverse strain gages. Bondable axial and transverse strain gages were used to evaluate the stress vs. strain relationship at lower strains because they are considerably more accurate at these levels than other instruments. The gages were mounted in the center of the reduced area of the specimen. Such gages typically debond at strains of 2 to 4%, rendering them ineffective at larger strain levels. A clip-on extensometer was used to measure axial strain to failure. This device is not as accurate as the strain gages at smaller strains, but provides for a reliable assessment of strain at larger values, specifically those beyond the initiation of plastic deformation.

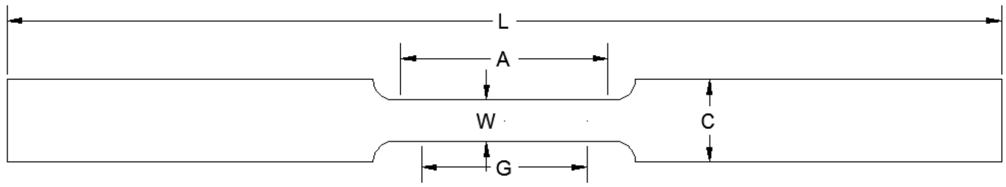

Sheet-Type, .5 in Wide	
Dimensions	*Length (in.)*
G - Gauge Length	2.00
W - Width	0.50
T - Thickness	
R - Radius	0.50
L - Overall Length	8.00
A - Length of Reduced Section	2.25
C - Width of Grip Section	1.00

Figure 2.1. Schematic of Tensile Coupon Specimen (ASTM – E8 2013)

Figure 2.2. Baldwin Testing Apparatus

2.3. Stress vs. Strain Data

The stress applied throughout the uniaxial tension test was computed by dividing the measured force by the original cross-sectional area of the tensile coupon. This strain generally is referred to as engineering strain. The uniaxial stresses vs. axial strains for all three specimens are shown in Figures 2.3 to 2.5. These plots show both the bondable strain gage and extensometer data. As illustrated in the figures, there is a local peak in stress near the end of the linear stress vs. strain data at about 0.0012 strain, after which there is a small stress reduction to a flat, or level, portion of the stress vs. strain plot. At a strain of about 0.025, there is a marked increase in stress with respect to strain.

An expanded view of the stress vs. strain data is shown in Figure 2.6, in which the combined strain gage and extensometer data were used to plot stress vs. strain within and beyond the elastic range. At the end of elastic range, locally variable readings were obtained with the bondable gages, and preference beyond this range was given to the extensometer data in developing the stress vs. strain relationship.

2.3.1. Young's Modulus and Yield Strength

Young's modulus was computed using the elastic range of the stress vs. strain curve and a combination of the bonded axial strain gage and extensometer data. These data are shown to a strain of 0.005 in Figure 2.6. Young's Modulus was determined by performing a linear regression for stress vs. strain from 3 ksi to 45 ksi (21 to 310 MPa). The yield strength, σ_y, was computed using the offset method, in which a line parallel to the linear part of the stress vs. strain plot is projected from 0.2% strain. The intersection of this line and the stress vs. strain curve provides an estimate of the yield stress for each specimen. The Young's modulus and yield stress for the specimens are presented in Table 2.1. The average Young's Modulus is 31500 ksi (217 GPa) with a standard deviation of 1260 ksi (8.89 GPa). The average yield stress is 44.8 ksi (309 MPa) with a standard deviation of 0.7 ksi (4.8 MPa).

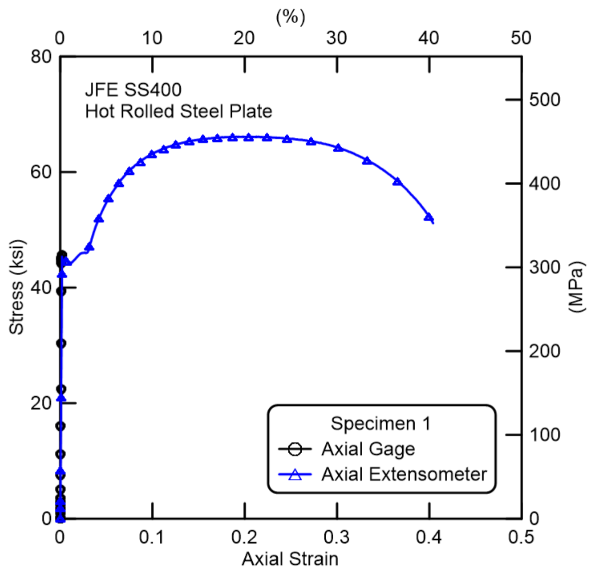

Figure 2.3. Stress – Strain Curve for Specimen 1

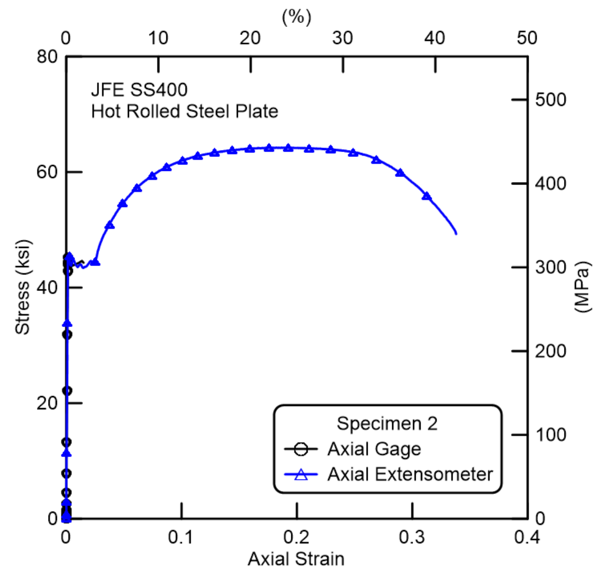

Figure 2.4. Stress – Strain Curve for Specimen 2

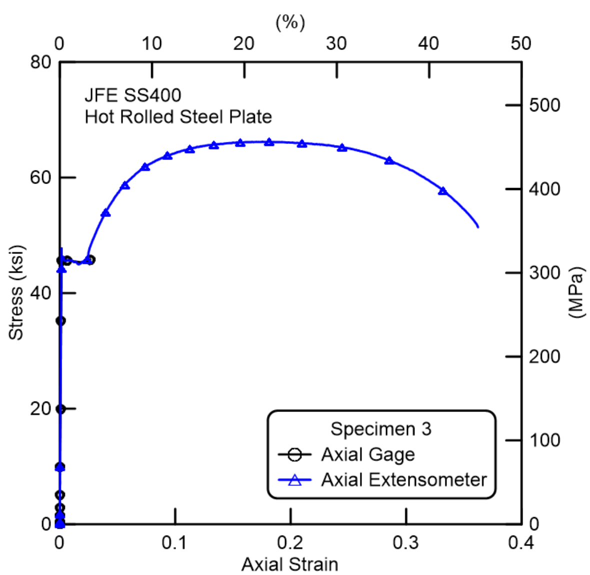

Figure 2.5. Stress – Strain Curve for Specimen 3

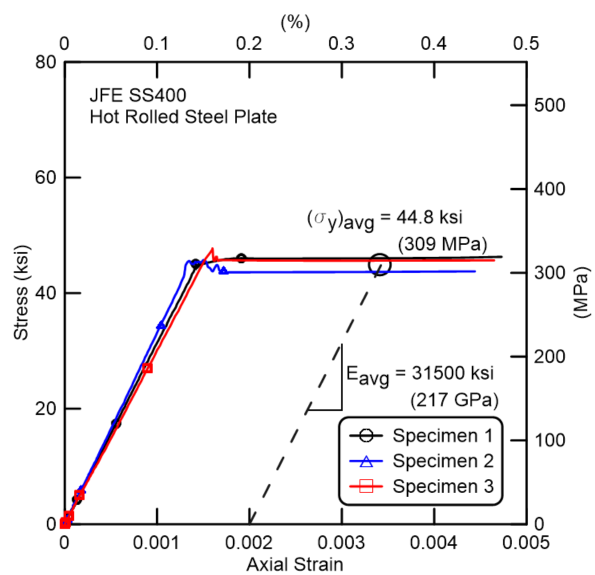

Figure 2.6. Average Young's Modulus and Yield Stress

Table 2.1. Young's Modulus and Yield Stress

Specimen	Young's Modulus, E ksi (GPa)	Offset Yield, σ_y ksi (MPa)
1	31,400 (216)	44.7 (308)
2	33,100 (228)	44.0 (303)
3	30,000 (207)	45.6 (314)
Average	31,500 (217)	44.8 (309)
Standard Deviation	1260 (9)	0.7 (4.8)

2.3.2. Ultimate Tensile Strength and Strain

Axial stress vs. strain data from the clip-on extensometers were used to determine the ultimate strength and strain, as shown in Figure 2.7. Table 2.2 gives the failure tensile stress and failure strain for these three specimens. The average ultimate stress was 65.5 ksi (452 MPa) with a standard deviation of 0.9 ksi (6 MPa). The average ultimate strain was 36.9% with a standard deviation of 2.7%

Table 2.2. Summary of Ultimate Tensile Stress and Strain

Specimen	Strength, ksi (MPa)	Strain (%)
1	66.1 (456)	40.3
2	64.2 (443)	33.8
3	66.2 (456)	36.5
Average	65.5 (452)	36.9
Standard Deviation	0.9 (6.2)	2.7

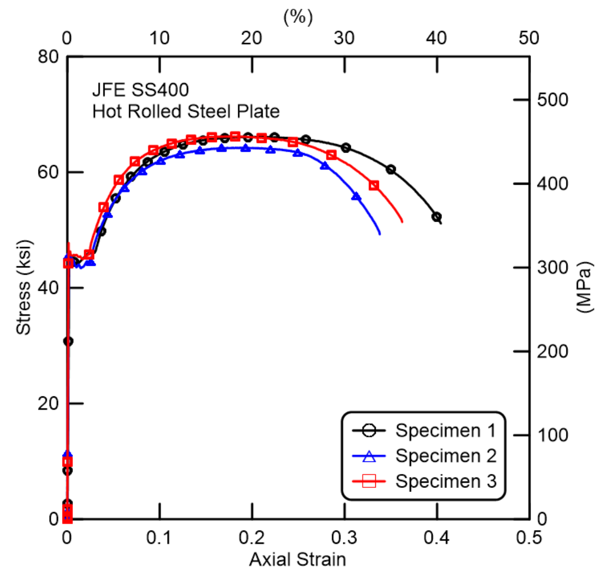

Figure 2.7. Stress - Strain Curve to Failure Using Clip-on Extensometer Data

2.3.3. Poisson's Ratio

Poisson's ratio, ν, is the negative ratio of transverse strain to axial strain for uniaxial loading. Poisson's ratio was derived from the transverse and axial strain gage data for stresses in the elastic range as shown in Figure 2.8. Poisson's ratio data are presented in Table 2.3 Poisson's ratio for all specimens was approximately 0.29 with a standard deviation of 0.02.

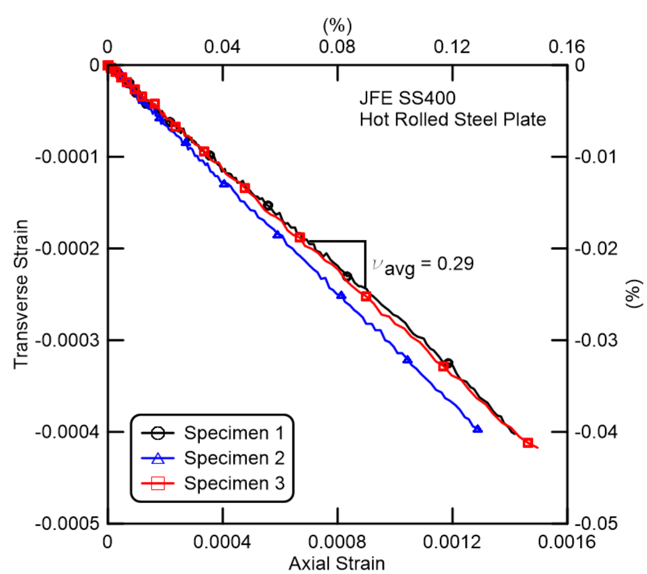

Figure 2.8. Transverse vs. Axial Strain in Elastic Range

Table 2.3. Poisson's Ratio Measured in Elastic Range

Specimen	Poisson's Ratio, ν
1	0.28
2	0.31
3	0.28
Average	0.29
Standard Deviation	0.02

2.4. Comparison of Test Results to JIS G3101, 2015 SS400

The uniaxial tension testing of hot rolled steel plate from JFE specimens was completed in accordance with the ASTM – E8 2013 Standard (ASTM, 2013). The yield stress, ultimate stress, Young's modulus, and Poisson's ratio are summarized in Table 2.4 and compared with the minimum specifications in the JIS SS400 Standard (JIS G3101, 2015). The yield and ultimate stresses are 26% and 13% greater than the minimum specifications, respectively.

Table 2.4. Comparison of Material Strengths to JIS G3101, 2015 SS400

Parameter	JFE	JIS G3101 SS400	Difference (%)
Yield Stress, ksi (MPa)	44.8 (309)	35.5 (245)	26
Ultimate Stress, ksi (MPa)	65.5 (452)	58-74 (400-510)	13
Young's Modulus, ksi (GPa))	31,500 (217)	-	-
Poisson's Ratio	0.29	-	-

Section 3

SPF Wave Compression Test

3.1. Introduction

This section summarizes the results of compression testing of the SPF wave feature developed by JFE. The compression test is designed to demonstrate wave performance under concentrated axial load and internal water pressure of typical supply systems.

The wave feature, as described in Section 1.2, is joined to lengths of straight pipe sections by welds. Shown in Figure 3.1, the straight sections of pipe are 35.8 in. (910 mm) long. Flanges were welded to each end of the straight pipe sections to which steel end caps with rubber gasket were bolted. The flange and end caps allow for pressurization of the specimen and a stiff mechanism for transferring axial force to the specimen.

3.2. Instrumentation

Figure 3.2 shows a plan view of the compression test setup and key instrumentation. An actuator and load cell were installed at the south end of the load frame to apply and measure compressive force, respectively. Four load cells were also used at the north end of the pipe to provide additional axial force measurements and to test and qualify the load measuring system used in the JFE split basin test. An electronic pressure transducer, located at the north end cap, measured internal water pressure during the test sequence.

Eight string potentiometers (string pots), mounted on the pipe at quarter points around the pipe circumference, were attached to the specimen and used to measure axial displacements along the specimen. As shown in Figure 3.3, string pots were fixed to the end flanges of the pipe and connected to support brackets located 4.3 in. (108 mm) south of the specimen centerline. Four string pots measured displacements across the south section of straight pipe while the other four measured displacements across the wave feature and north section of straight pipe.

A total of 20 strain gages were fixed to the exterior of the specimen at three planes, designated as ST-20, ST0, and ST+20, as shown in Figure 3.1 and Figure 3.2. At each plane the gages were located at the 12, 3, 6, and 9 o´clock positons (crown, east springline, invert, and west springline, respectively). Gage plane ST+20 was positioned 20.5 in. (520 mm) north of the wave feature and included four gages oriented in each of the axial and circumferential directions. Plane ST-20 was positioned 20.5 in. (520 mm) south of the wave feature and included four axial gages. An additional plane ST0 was centered on the wave and included four axial and four circumferential gauges. The instrument locations and gage names are listed in Table 3.1.

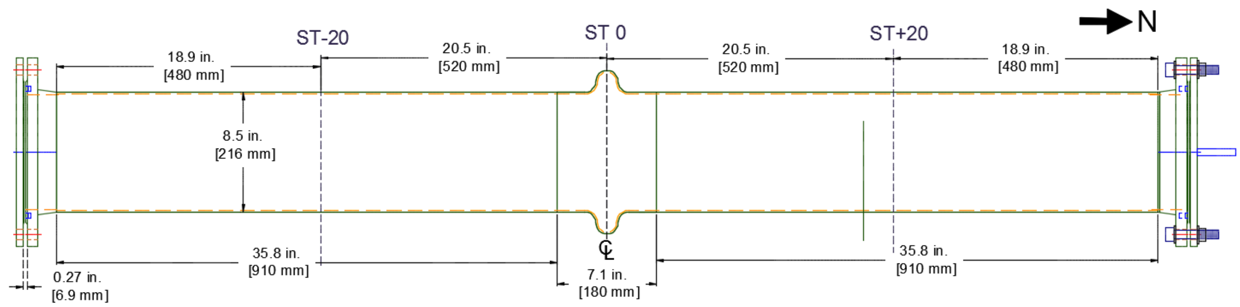

Figure 3.1. Compression Test specimen with SPF Wave Feature

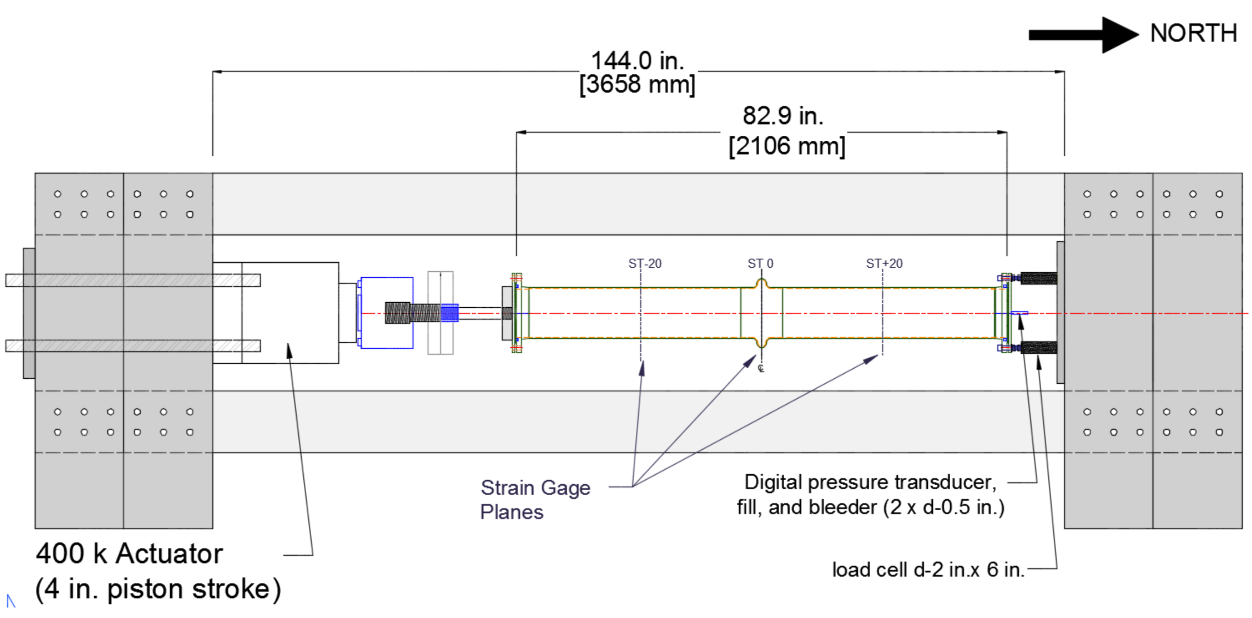

Figure 3.2. Plan View of Axial Compression Test

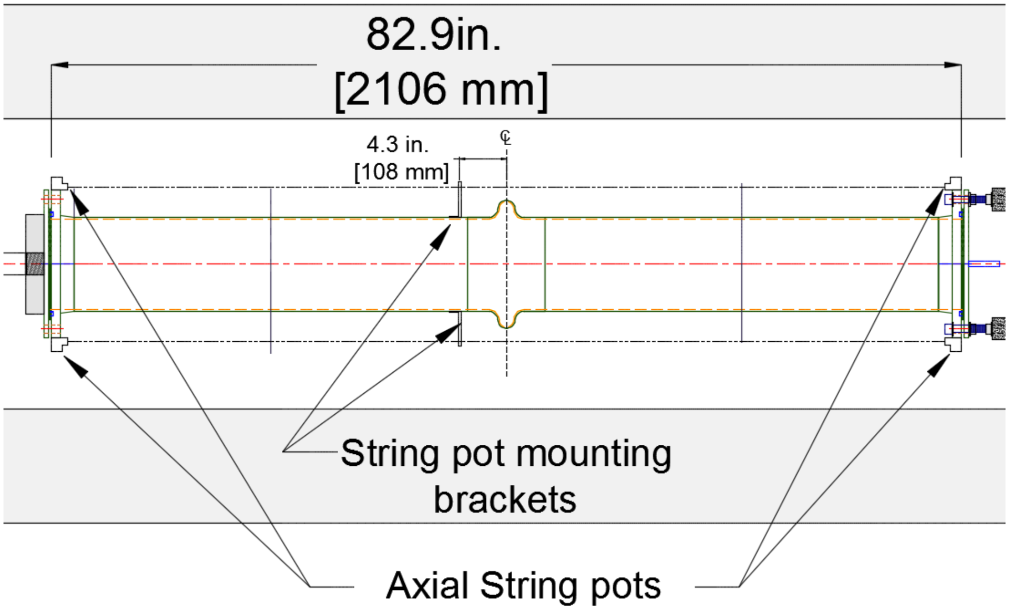

Figure 3.3. Compression Test Specimen with Positon of Axial String Potentiometers

Table 3.1. Instrumentation for JFE SPF Compression Test

Location	Instrument	Local Instrument Name
20.5 in. North of SPF	East Springline, Axial Strain	ST+20EA
20.5 in. North of SPF	East Springline, Circumferential Strain	ST+20EC
20.5 in. North of SPF	Crown, Axial Strain	ST+20CA
20.5 in. North of SPF	Crown, Circumferential Strain	ST+20CC
20.5 in. North of SPF	West Springline, Axial Strain	ST+20WA
20.5 in. North of SPF	West Springline, Circumferential Strain	ST+20WC
20.5 in. North of SPF	Invert, Axial Strain	ST+20IA
20.5 in. North of SPF	Invert, Circumferential Strain	ST+20IC
20.5 in. South of SPF	East Springline, Axial Strain	ST-20EA
20.5 in. South of SPF	Crown, Axial Strain	ST-20CA
20.5 in. South of SPF	West Springline, Axial Strain	ST-20WA
20.5 in. South of SPF	Invert, Axial Strain	ST-20IA
North Side of SPF	String Pot, East Springline	N-Disp-E
North Side of SPF	String Pot, Crown	N-Disp-C
North Side of SPF	String Pot, West Springline	N-Disp-W
North Side of SPF	String Pot, Invert	N-Disp-I

Table 2.2. Instrumentation for JFE SPF Compression Test (completed)

South Side of SPF	String Pot, East Springline	S-Disp-E
South Side of SPF	String Pot, Crown	S-Disp-C
South Side of SPF	String Pot, West Springline	S-Disp-W
South Side of SPF	String Pot, Invert	S-Disp-I
North End	Northeast Top Load Cell	NE-Top
North End	Northwest Top Load Cell	NW-Top
North End	Northwest Bottom Load Cell	NW-Bottom
North End	Northeast Bottom Load Cell	NE-Bottom
Actuator	Load Cell	Interface Load
Actuator	Displacement	Act Disp.
Internal Pressure	Pressure Transducer	Pressure

1 in. = 25.4 mm

3.3. Test Sequence

After the specimen was instrumented and centered in the test frame the test sequence was initiated by starting the data acquisition system and laboratory hydraulic systems. The data sampling rate was 5 Hz. The north end load cells, mounted on bolts, were slowly tightened bringing the specimen in contact with the southern load cell/actuator. The north load cells were adjusted to about 125 lb (0.56 kN) each, totaling 500 lb (2.22 kN) of axial load prior to application of internal pressure. These adjustments ensured concentric initial loading conditions and restrained the pipe from axial movement due to internal pressure. Approximately 80 psi (550 kPa) of internal water pressure was applied. The measuring systems were checked and an initial actuator displacement of 3.7 in. (94 mm) was applied.

The actuator used for this test has a compressive load capacity of 400 kips (1780 kN) and stroke of 4 in. (200 mm). Following the initial displacement step, the specimen was unloaded and depressurized, and the actuator was retracted. The specimen was then repositioned to apply a second loading increment to a total imposed axial displacement of 6.4 in. (163 mm).

3.4. Experimental Results

In this section the test measurements will be presented, followed by the summary results of the force-displacement response for the SPF wave feature. Figure 3.4 shows the test specimen mounted in the compression test frame. Figure 3.5(a) – (d) show photographs of the compression test setup and the deformed SPF wave at 0, 0.5, 2, and nearly 4 in. (0, 13, 50 and 100 mm) of compressive displacement.

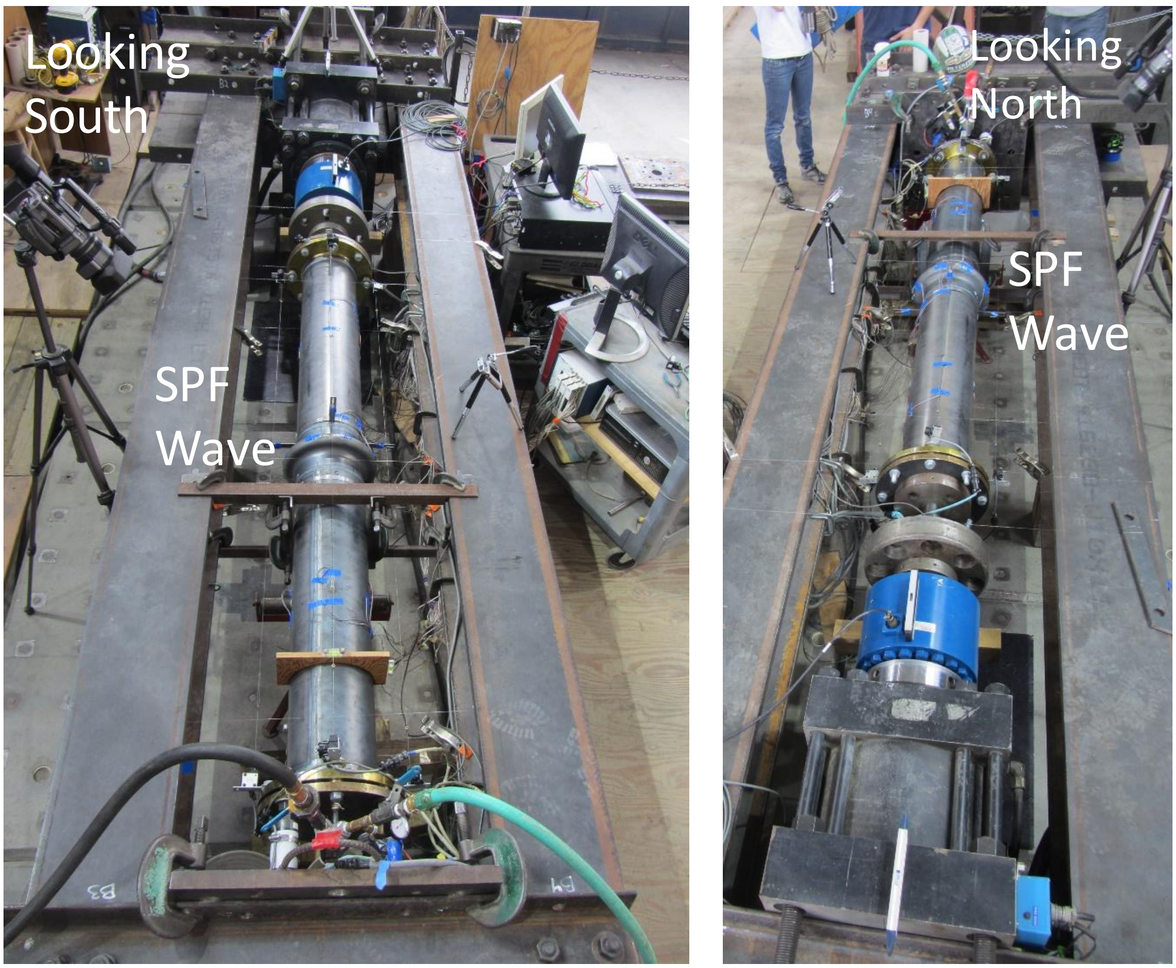

Figure 3.4. Test Apparatus and SPF Specimen in the Compression Frame

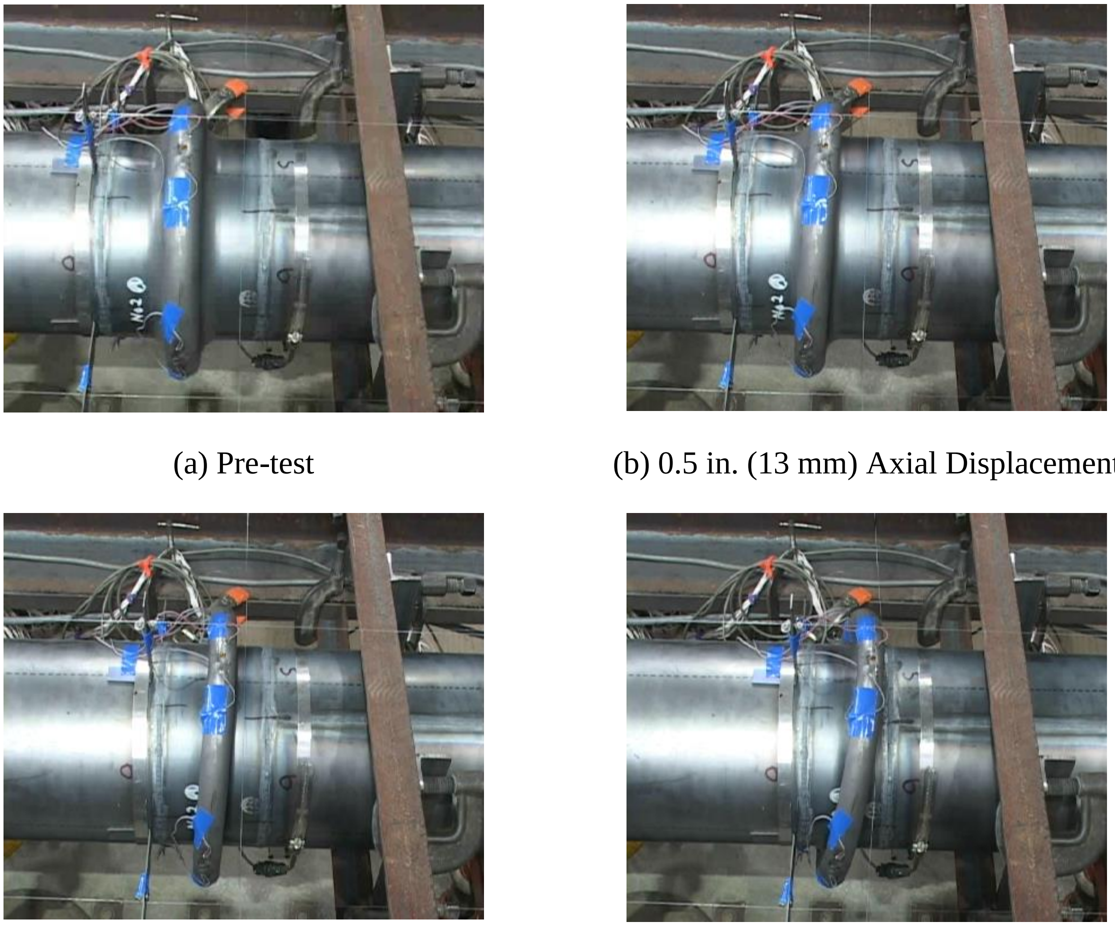

(a) Pre-test

(b) 0.5 in. (13 mm) Axial Displacement

(c) 2 in. (50 mm) Axial Displacement

(d) 3.7 in. (94 mm) Axial Displacement

Figure 3.5. SPF at Several Compressive Deformation Levels

3.4.1. Displacements

The test was performed under displacement control using the servo-hydraulic actuator at the south end of the test frame. Compression was applied by the actuator in two discrete steps. The actuator had a range of 3.7 in. (94 mm.) for this test. After the full range of the actuator was reached, the actuator was retracted, additional spacers placed between the load cell at the end of the actuator and the pipe end cap, and additional compression displacements were applied to the specimen. The actuator axial displacement vs. (arbitrary) time is shown in Figure 3.6. The time increments for the initial compression load, repositioning of the actuator, and additional load application are identified. The initial 3.7 in. (94 mm) of compressive displacement was applied over an 8 min.

duration. The specimen and actuator were then repositioned. The second application of actuator displacement over an additional 6 min. resulted in a total of 6.4 in. (162 mm) of actuator movement. Actuator displacement is a direct measurement of piston movement. Axial displacements of the specimen were also measured by string potentiometers.

Figure 3.7 shows the average north and south string pot measurements vs. actuator displacement. The north string pots clearly show the greatest movement while the south end of the test specimen behaves as a nearly rigid pipe section with minor elastic shortening. There is some small offset displacement at the beginning of the north pot displacements, on the order of 0.1 in. (2.5 mm). The south pots show nearly zero displacement until near the end of the actuator stroke. The wave feature deformations were accompanied by deformation of the south pot attachment bracket during the second phase of displacement. As a result, the south pot displacements during this phase of the test are not reliable and are not reported after 3.46 in. (87.9 mm) of wave compressive displacement.

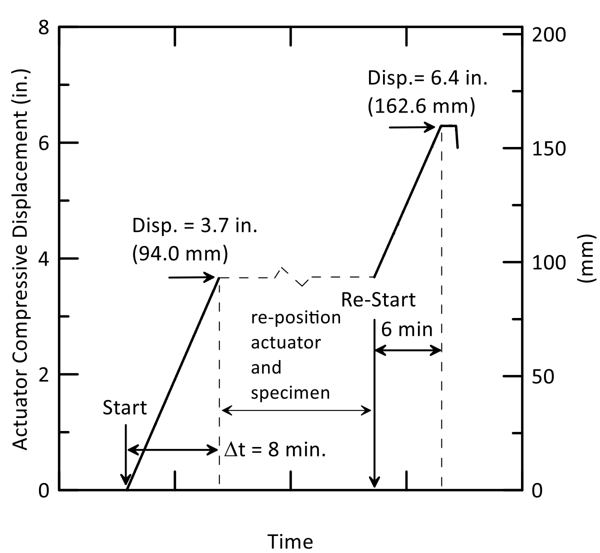

Figure 3.6. Actuator Compressive Displacement vs. Time

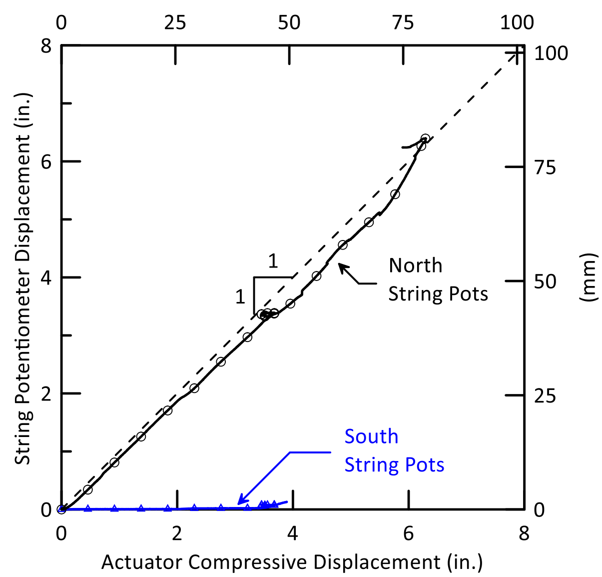

Figure 3.7. Actuator Compressive Displacement vs. String Potentiometer Displacements

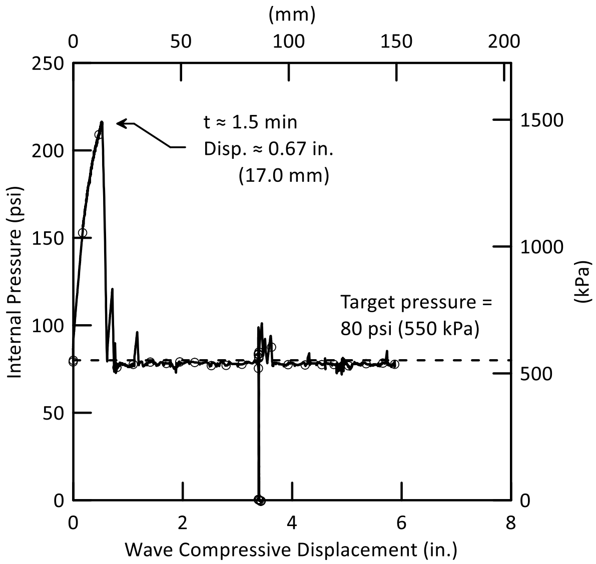

Figure 3.8. Pipe Internal Pressure vs. Actuator Compressive Displacement

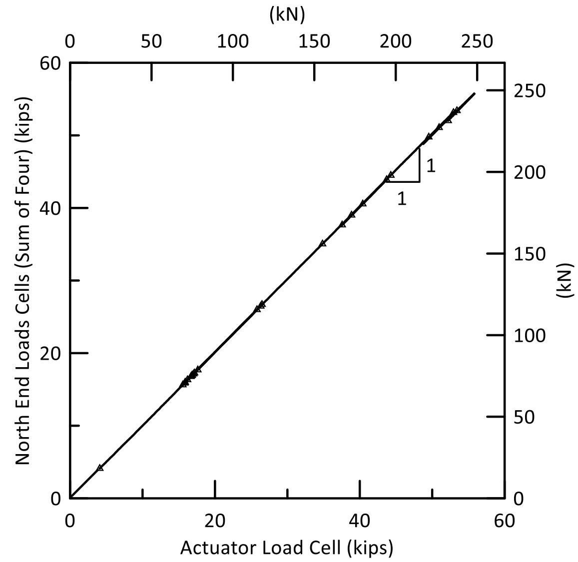

Figure 3.9. North End Load Cell vs. South End Actuator Load Cell Measurements

3.4.2. Internal Pressure

The internal pressure during the compression test is shown relative to time in Figure 3.8. The test plan intention was to keep the internal pressure at 80 ± 10 psi (550 ± 70 kPa). However, during the initial loading stage the pressure release mechanism for water pressure did not function properly, causing internal pressure levels to increase significantly in response to volume reduction in the pipe. A maximum internal pressure of 213 psi (1470 kPa) occurred at an actuator displacement of 0.67 in. (17.1 mm). At that time (roughly 1.5 min. into the compression test) the pressure was manually reduced to 80 psi (550 kPa) without interrupting loading. At 3.7 in. (94 mm) the specimen was depressurized during adjustments for the second loading cycle.

3.4.3. Axial Loads

The axial force, which is presented as the sum of the four north load cell measurements, is plotted in Figure 3.9 relative to the load cell measurements at the south actuator. These loads, which were measured at the south and north ends of the test specimen, respectively, are nearly identical. Pipe loads in the split basin test were recorded using multiple load cells similar to the ones used in this test. These results provided confirmation that multiple load cells can be recorded effectively and summed to determine the pipe end reaction.

3.4.4. Pipe Strains

Strain gage results are presented for the axial and circumferential strain gages at the north and south midpoints of the pipe. The gage measurements were used to provide a redundant measuring system for applied pipe forces, and to assess the influence of internal pressure on the combined loading of the pipe. They are not used in this report to evaluate the pipe yield response and detailed nonlinear behavior of the SPF feature.

Figure 3.10 shows the average axial strains at the north and south gage planes with the circumferential (hoop) strains at the north gage plane. The north and south axial strains are virtually identical. Both the axial and circumferential strains show some strain at zero displacement. These initial strains of about $\varepsilon_{axial} \approx -30\ \mu\varepsilon$ and $\varepsilon_{hoop} \approx 150\ \mu\varepsilon$ are due to initial internal pressurization. The peak circumferential strain measured at about 19 mm (0.75 in.) of axial displacement correlates with the increase in internal pipe pressure, as shown in Figure 3.8.

3.4.5. Wave Displacements

The actuator, string pot, and axial strain gage measurements can be used to evaluate the movements directly across the wave feature. The axial strains measured at the midpoint of the straight pipe sections can be multiplied by the distance between the SPF wave welds and end caps [a distance of 35.8 in (909 mm) as indicated in Figure 3.2] to approximate the elastic shortening due to "strain displacement" of the specimen outside the wave feature. The maximum displacements calculated are less than 0.03 in. (0.8 mm) for both the north and south sections. The total shortening of the test specimen is represented by the sum of the north and south string pots. This shortening is similar but not the same as the actuator displacement. As shown earlier in Figure 3.7, there is some small initial discrepancy between the string pot and actuator displacements arising from deformation in the compression test frame and seating load adjustments.

Subtracting the calculated "strain displacements" from the sum of the north and south string pot measurements represents the compression across the SPF wave, which is referred to as the wave displacement. At the end of the first load step the wave displacement results in a total compression of 3.46 in. (87.9 mm), compared to the actuator displacement of 3.67 in. (93.2 mm.), with a difference of 0.21 in. (5.3 mm) as depicted in the Figure 3.11.

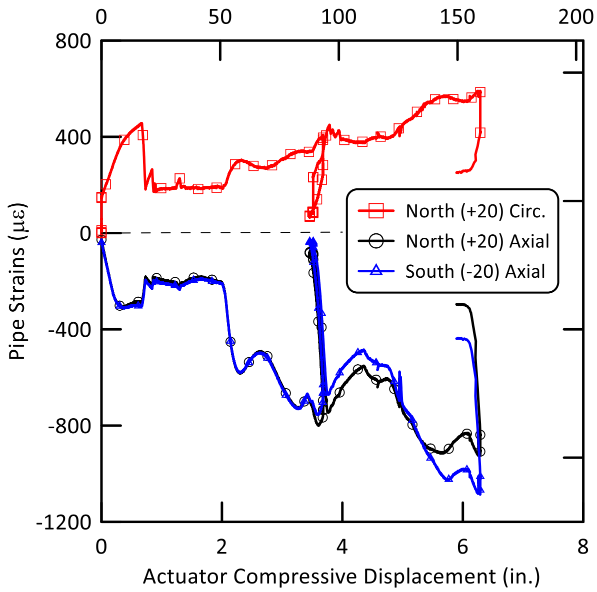

Figure 3.10. Pipe Strains at North and South Gage Planes

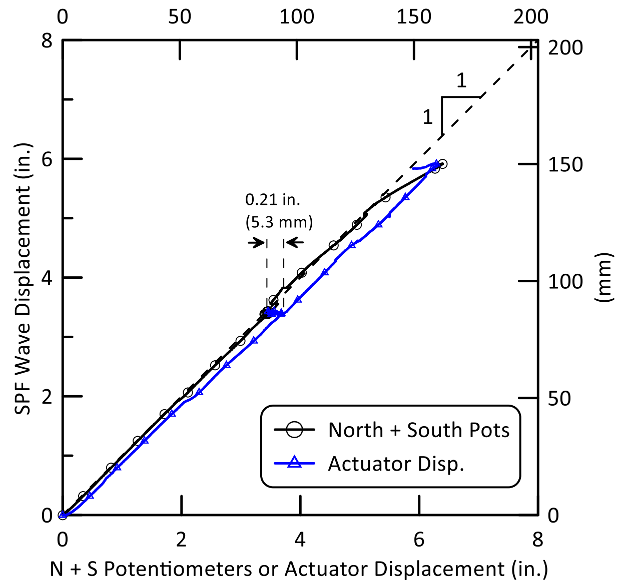

Figure 3.11. Wave Displacements vs. String Pot and Actuator Displacements

3.4.6. SPF Wave Feature Axial Force-Displacement

The force – displacement results for the SPF wave feature are shown in Figure 3.12. The wave displacements are the string pot measurements adjusted by the elastic shortening of the straight pipe sections, as described previously. The force measurements are those of the hydraulic actuator, which are the same as those measured at the north end load cells. The end forces have been corrected for the effects of pipe internal pressure. At a displacement of approximately 0.21 in. (5.3 mm) the pipe force was 17.9 kips (79.6 kN). The load then dropped to about 13 kips (57.8 kN) at a displacement of 1.86 in. (47.2 mm). At this displacement the wave feature had closed, and metal-to-metal contact at the base of the wave led to increasing load with additional axial displacement. The unloading-reloading can be seen at approximately 3.4 in. (86.4 mm) of wave displacement, at which point the specimen and actuator were adjusted for further loading.

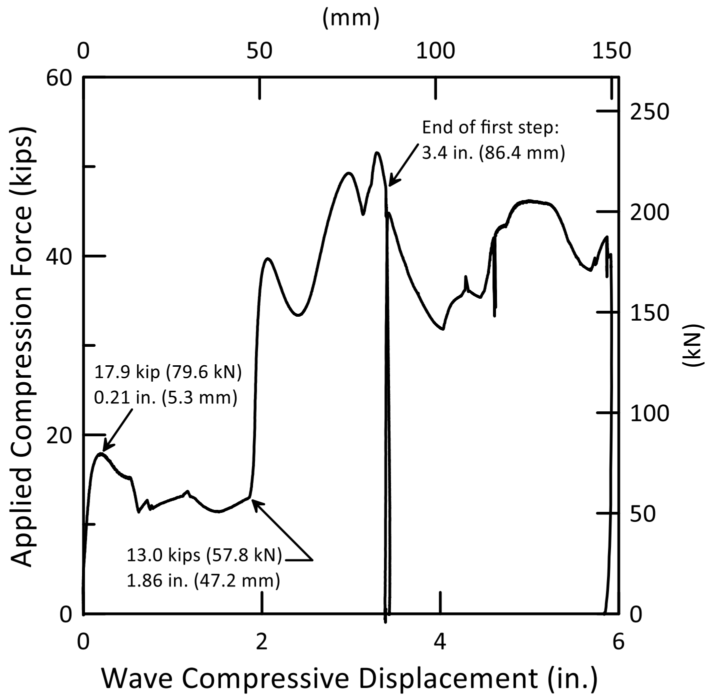

Figure 3.12. SPF Wave Feature Compressive Force – Wave Displacement Response

3.4.7. SPF Wave Strains

Axial and circumferential strain gage rosettes were placed on the center of the wave feature at the quarter points as requested by JFE. Table 3.2 provides the location, orientation, and designation of longitudinal and circumferential gages at the wave feature. As expected, the strains at the wave feature are much greater than those measured on the adjoining pipe sections.

Figure 3.13(a) shows the axial strains at the wave to a wave displacement of approximately 4 in. (102 mm). Figure 3.13(b) shows the strains to a maximum wave displacement of 6 in. (153 mm) as the test was continued after re-positioning the specimen and the actuator. Figure 3.13 shows that the axial strains at the wave are initially compressive, and then become increasingly tensile as the wave deforms to 1.86 in. (47.2 mm) of compressive wave displacement. In Figure 3.12 the compressive force increases rapidly beyond 1.86 in. (47.2 mm), due most likely to metal-to-metal contact at the base of the wave. At this point, there is a sharp decrease in the axial strains. Figures 3.14(a) and (b) show a similar but more subdued peaking of hoop strain at approximately 1.86 in.

(47.2 mm) of compressive wave displacement for the circumferential gages mounted directly on the wave feature.

Table 3.2. Strain Gages on SPF Wave Feature

Location and Orientation	Designation
East Springline, Axial Strain	ST0EA
East Springline, Circumferential Strain	ST0EC
Crown, Axial Strain	ST0CA
Crown, Circumferential Strain	ST0CC
West Springline, Axial Strain	ST0WA
West Springline, Circumferential Strain	ST0WC
Invert, Axial Strain	ST0IA
Invert, Circumferential Strain	ST0IC

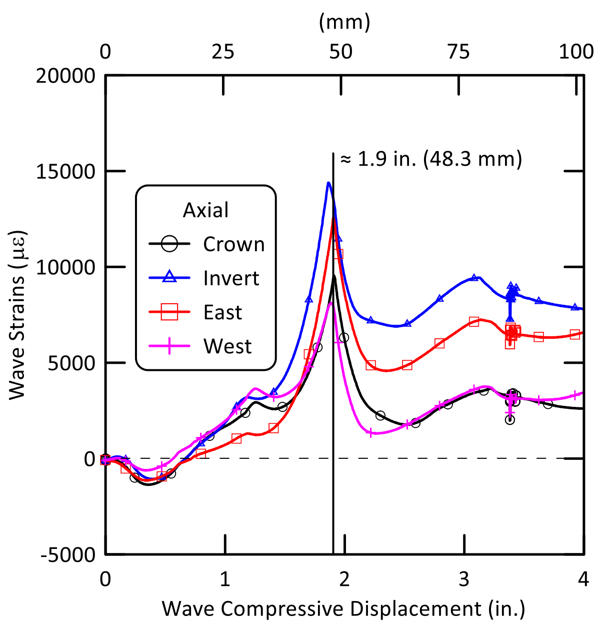

(a) Up to 4 in. Wave Displacement

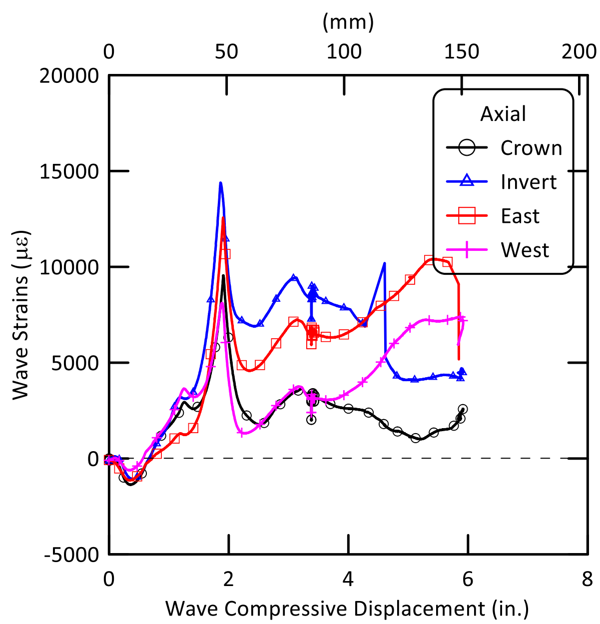

(b) Entire Test

Figure 3.13. Axial Strains at SPF Wave Feature

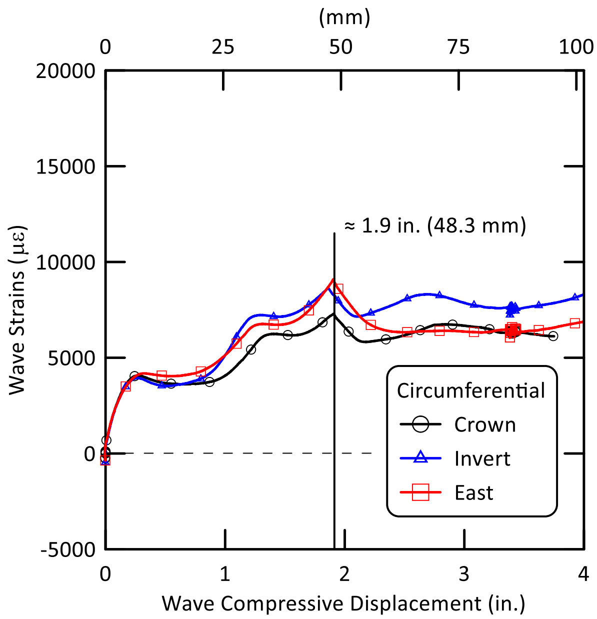

(a) Up to 4 in. Wave Displacement

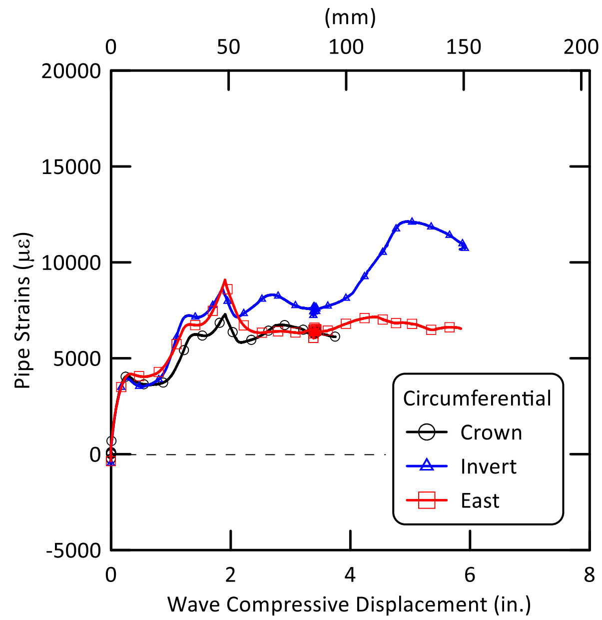

(b) Entire Test

Figure 3.14. Circumferential (Hoop) Strains at SPF Wave Feature

3.4.8. Post-test Images of Wave Feature

Additional photographs of the SPF wave feature are provided in Figure 3.15. These photographs show the extent of buckling and deformation of the specimen at the end the test at the crown, springline, and invert relative to the wave feature in its pre-test condition. The images show the full extent of wave deformation under significant loading three times greater than the intended design value.

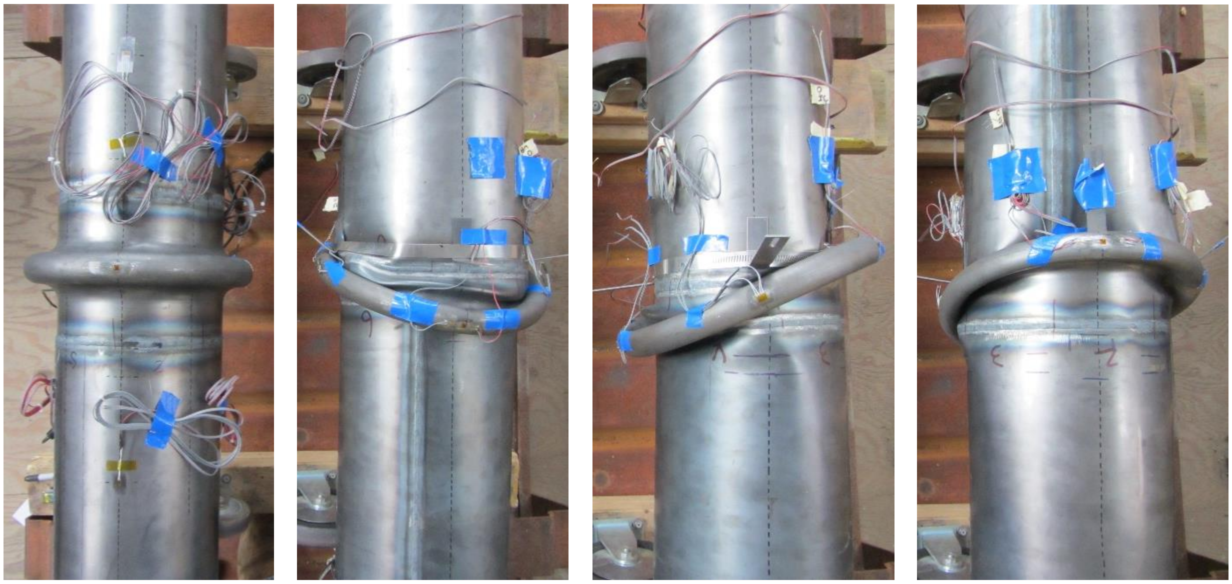

(a) Pre-test (b) Crown (c) Springline (d) Invert

Figure 3.15. Pre- and Post-Test Photos of SPF wave feature

3.5. Compression Test Conclusions

A compression test was performed on a 6.6-ft (2 m)-long section of SS 400 pipe with a JFE wave feature at its midpoint. The pipe was pressurized with water to at least 80 psi (550 kPa) throughout the test. An initial actuator displacement of 3.7 in. (94 mm) was applied, the pipe section and loading system adjusted, and an additional 2.7 in. (69 mm) displacement applied. The wave feature experienced significant deformation without rupture or reduction of internal pressure.

At a wave displacement of 0.21 in. (5.3 mm) the pipe reached a peak force of 17.9 kip (79.6 kN), after which the force decreased until a wave displacement of roughly 1.86 in. (47.2 mm). At this point the wave feature closed and the pipe compressive force increased. At no point during the test did the pipe rupture or lose pressure. The test was continued until a wave displacement of approximately 6 in. (152 mm) without loss of pressure.

Section 4
SPF Wave Bending Test

4.1. Introduction

This section summarizes the results of the four-point bending testing of the SPF wave feature developed by JFE. The material and geometry of the wave are as described previously. The wave feature is joined to lengths of straight pipe sections by welds. Figure 4.1 shows a profile view of the test setup including dimensions of the test specimen. Flanges were welded to each end of the straight pipe sections to which steel end caps with rubber gaskets were bolted. The flange and end caps allow for pressurization of the specimen.

4.2. Setup and Instrumentation

Figures 4.1 and 4.2 show profile views of the test setup. A Baldwin test frame with 400 kip (1780 kN) capacity and 12 in. (300 mm) stroke was used for this test. Support points were positioned at 60 in. (1500 mm) on either side of the wave feature, centered in the test frame. Loading points were located at 24 in. (600 mm) on either side of test centerline. Specially designed support saddles, shown in Figure 4.3, were used at each of the four contact points to distribute stress and prevent local deformation and ovaling of the specimen as well as provide an adequate surface for roller interaction.

Applied load and displacements were recorded throughout the test sequence. An electronic pressure transducer, located at the north end cap, measured internal water pressure.

Also shown in Figure 4.1 are the eight string potentiometers (string pots) used to measure vertical displacements along the specimen. String pots were fixed to the invert of the specimen at symmetric distances of 4, 24 and 48 in. (100, 600, and 1200 mm) from the center of the setup. Two additional string pots were attached to the east and west springline of the wave feature to provide a measure of vertical displacement at the center of the test setup. The instrument locations and names are listed in Table 4.1.

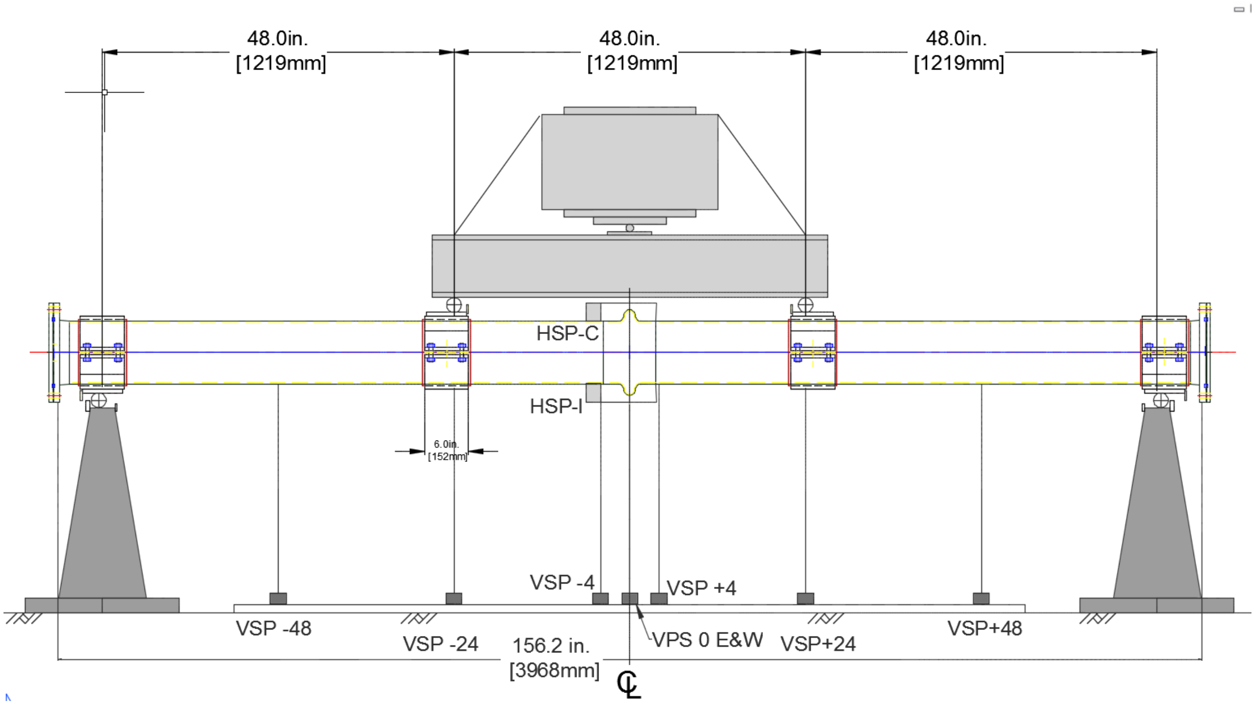

Figure 4.1. Bending Test Specimen with Wave Feature Showing String Potentiometer Locations

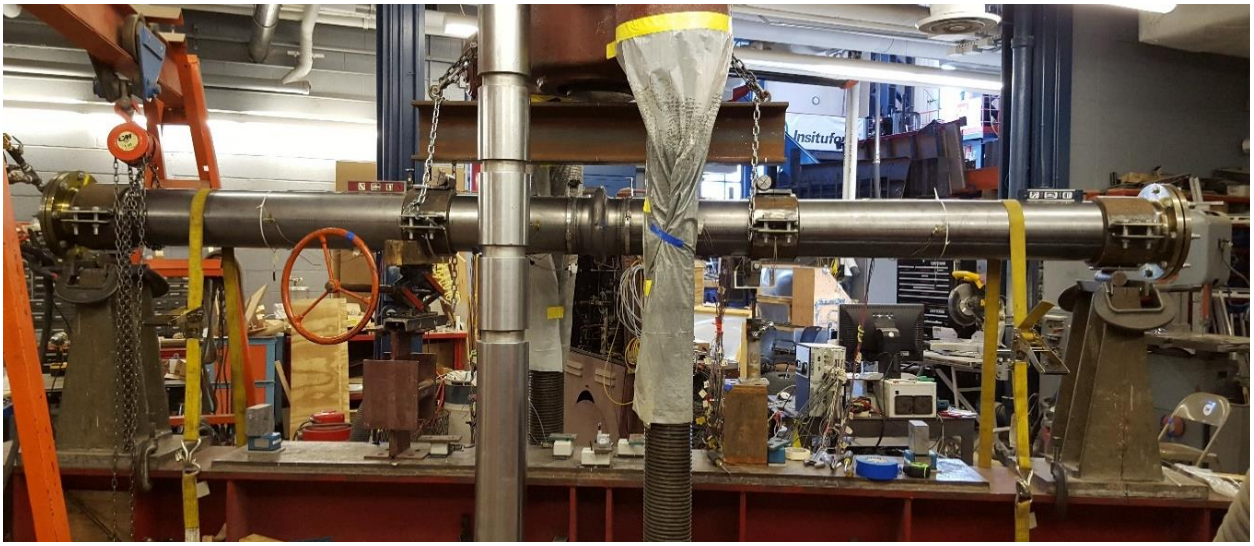

Figure 4.2. Profile View of Four-point Bending Test

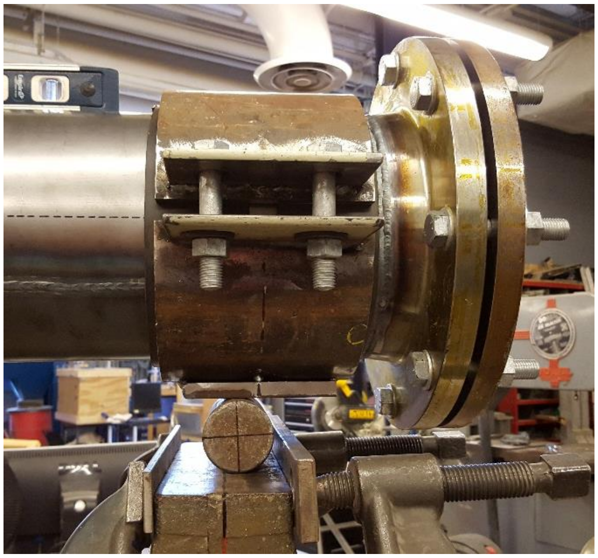

(a) Support Saddle and Roller at Support Point before Loading

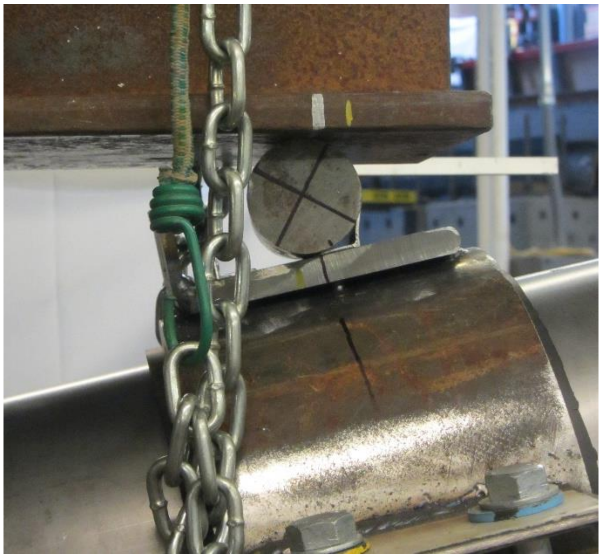

(b) Loading Saddle and Roller at Loading Point during Bending Test

Figure 4.3. Support and Loading Saddles for Bending Tests

Table 4.1. Instrumentation for JFE SPF Compression Test

Location	Instrument Description	Instrument Name
Test Frame	400K Baldwin Test Frame	Load
North End Cap	Pressure Transducer	Pressure
48 in. north of center	Vertical String Pot, invert	VSP+48
24 in. north of center	Vertical String Pot, invert	VSP+24
4 in. north of center	Vertical String Pot, invert	VSP+4
Center of wave	Vertical String Pot, east springline	VSP 0E
Center of wave	Vertical String Pot, west springline	VSP 0W
4 in. south of center	Vertical String Pot, invert	VSP-4
24 in. south of center	Vertical String Pot, invert	VSP-24
48 in. south of center	Vertical String Pot, invert	VSP-48
center, across wave	Horizontal String Pot, crown	HSP-C
center, across wave	Horizontal String Pot, invert	HSP-I
Test Frame	Vertical String Pot	Table Disp.

1 in. = 25.4 mm

4.3. Test Sequence

After the specimen was instrumented, filled with water, and centered in the test frame the test sequence was initiated by starting the data acquisition system and load frame hydraulic system. The data sampling rate was 2 Hz. The load table was raised approximately ¼ in. (6 mm) to allow vertical load measurement. The specimen was then pressurized to approximately 80 psi (550 kPa) and manually adjusted during the test be with in ±10 psi (70 kPa) of the initial value. Jacks supporting the center of the specimen were slowly lowered and removed. The table was raised until the spreader beam came in contact with the loading points (rollers). Adjustments were made to the position of the spreader beam and rollers to ensure symmetric loading conditions.

The maximum test frame stroke was 12 in. (300 mm), so the test was performed in two steps to reach the final level of deformation. Load was applied to the test specimen until a table displacement of approximately 11.5 in. (290 mm). The specimen was then unloaded, frame crosshead adjusted, and loading resumed until maximum deformation was reached.

4.4. Experimental Results

The following section provides results from the JFE four-point bending test. Measurements of vertical displacement, applied load, internal water pressure, and wave rotation are reported, followed by the moment-rotation relationship for the SPF wave feature.

4.4.1. Vertical Displacements

Vertical displacement was applied by the test frame in two discrete steps. The load frame used for this test had a range of about 12 in. (300 mm). After the full range of the load frame was reached the table was returned to its initial position, load frame crosshead was lowered, and additional vertical displacement were applied to the specimen. The vertical table displacement vs. time is shown in Figure 4.4. The initial loading sequence occurred during the first 1800 seconds followed by a pause before the table was retracted. The maximum imposed vertical displacement of the table during this stage was 11.5 in. (290 mm). The second loading sequence began at approximately 3200 seconds. This sequence imposed an additional 5.2 in. (132 mm) of vertical displacement. Table displacement was paused at 3800 seconds and retracted at about 4000 seconds.

Figure 4.5 shows the vertical spring pot (VSP) displacements measured along the pipe at four increments of imposed table displacement. The figure shows very good agreement between string pots positioned symmetrically on either side of the test centerline. The continuous progression of these displacements indicates that the assumption of rigid body movement either side of the wave can be used to determine rotation at the wave.

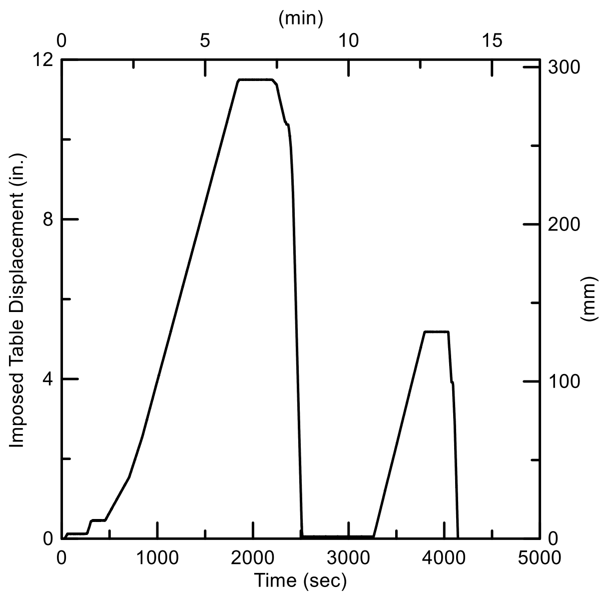

Figure 4.4. Vertical Table Displacement vs. Time

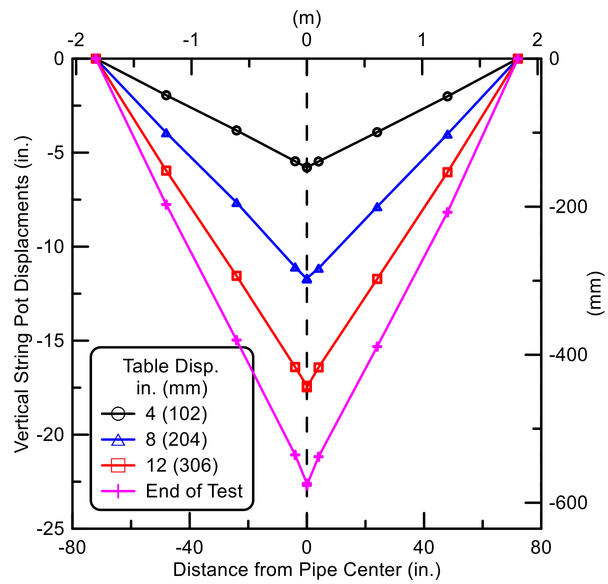

Figure 4.5. Vertical String Pot Measurements along Specimen at Various Levels of Imposed Displacement

4.4.2. Applied Load

The load applied and measured by the Baldwin test frame is shown relative to time in Figure 4.6. The two loading sequences can be clearly identified. The initial variation in load measured during the first 500 seconds of the test represents positioning of the 250 lb (1.1 kN) load spreader beam. This load increase corresponds to initial table displacements shown in Figure 4.4. A knee in the load data at around t = 1000 seconds represents a reduction in bending stiffness. The momentary drop in load at t = 3600 sec correlates with a minor translation [< 0.5 in. (12 mm)] of the north support roller. The first and second load sequences reach maximum load values of 3.81 and 3.95 kips (16.9 and 17.6 kN), respectively.

4.4.3. Internal Pressure

Figure 4.7 shows internal pipe pressure vs. time for the duration of the bending test. Initial pressure was manually adjusted during loading to remain generally within ±10 psi (70 kPa) of the target internal pressure, 80 psi (550 kPa). The dip in pressure at t = 2300 sec is a result of specimen unloading and repositioning. While fluctuations in internal pressure occurred due to changes in internal volume during bending, no signs of leakage were observed or measured at any time during the test.

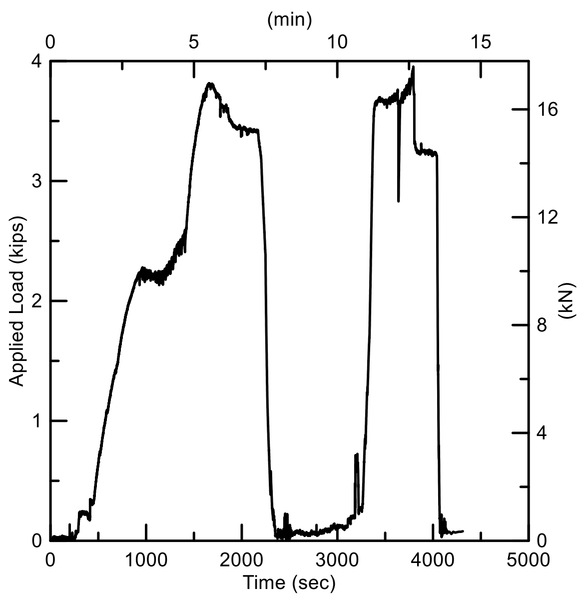

Figure 4.6. Applied Load vs. Time

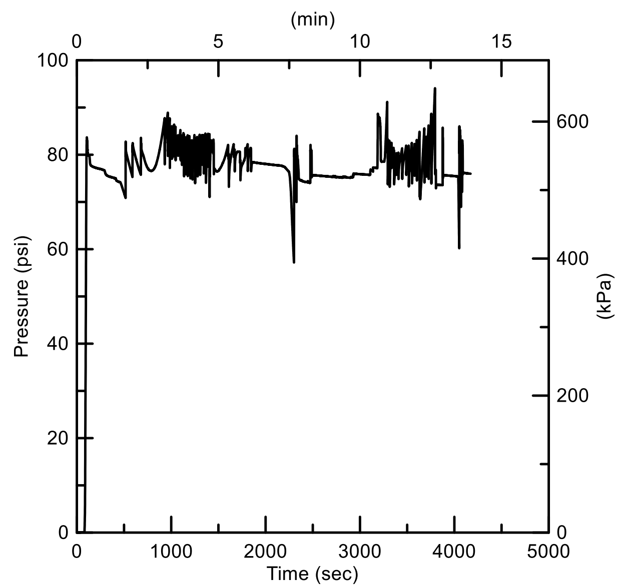

Figure 4.7. Internal Pressure vs. Time

4.4.4. Wave Rotations

Rotation (or deflection) of the wave feature was determined from vertical string pot (VSP) measurements. The straight sections of pipe welded to either side of the wave remained linear throughout the test. Bending deformation was concentrated in the immediate vicinity of the wave. Rotations can be calculated as the arcsine of vertical string pots (VSP) displacement divided by the distance from the support. Figure 4.8 plots the wave rotation vs. time. Each line represents the sum of rotations calculated from VSPs located at equal distances either side of the wave. The rotations shown in Figure 4.8 are calculated based on the distance from the VSP to the roller support. For example, the rotation angle of the right side of the specimen from the VSP at 0 to the roller support on the right at a distance of 72 in. (1829 mm) was calculated and the rotation from VSP 0 to the left roller support was determined. Then, these rotations were added together to determine the rotational angle in the bending test. The figure shows very close agreement among the rotation measurements, providing further evidence that the straight sections of pipe remained linear throughout loading.

Figure 4.9 shows measurements recorded by horizontal string pots (HSP) located at the crown (top) and invert (bottom) of the wave vs. average wave rotation measured from VSPs. These devices, shown in Figure 4.10, measure across the wave at locations about 3.5 in. (90 mm) from the either side of the wave centerline. At the start of the test the string pot and fixed point were located approximately 6.5 in. (165 mm) above and below the specimen springline. Initially opening at the invert of the wave occurred at a greater rate than wave closure at the crown. After 10 degrees of rotation this trend reversed, and compression at the crown occurred more rapidly with each increment of joint rotation.

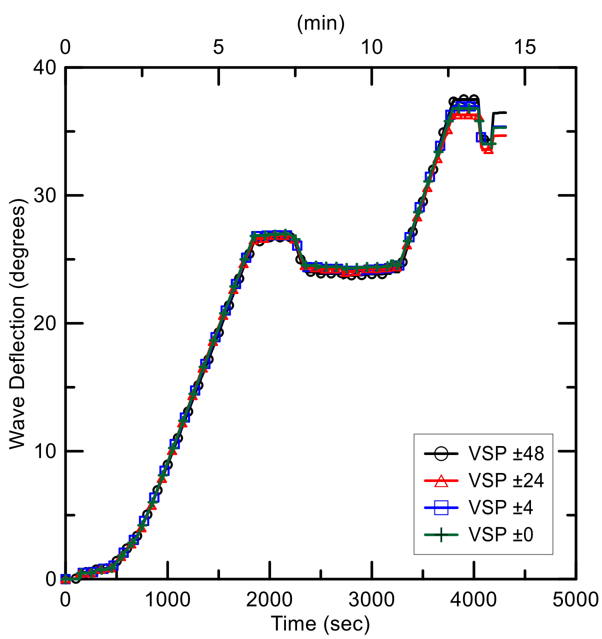

Figure 4.8. Wave Rotation Calculated from Individual Vertical String Pots

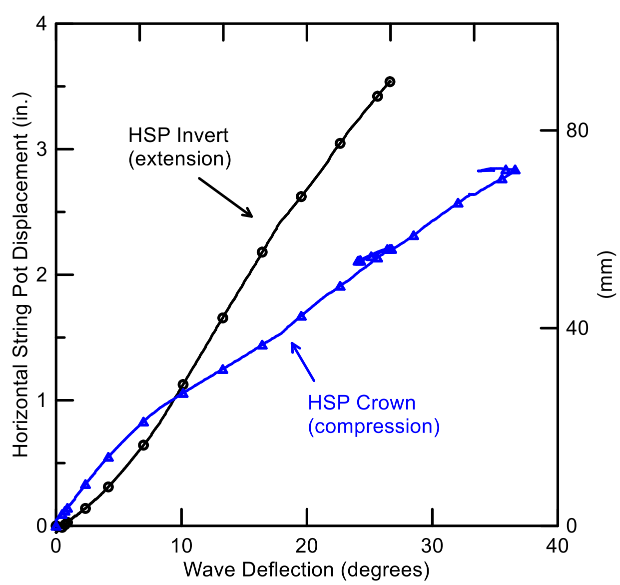

Figure 4.9. Horizontal Displacement at Crown and Invert of Wave

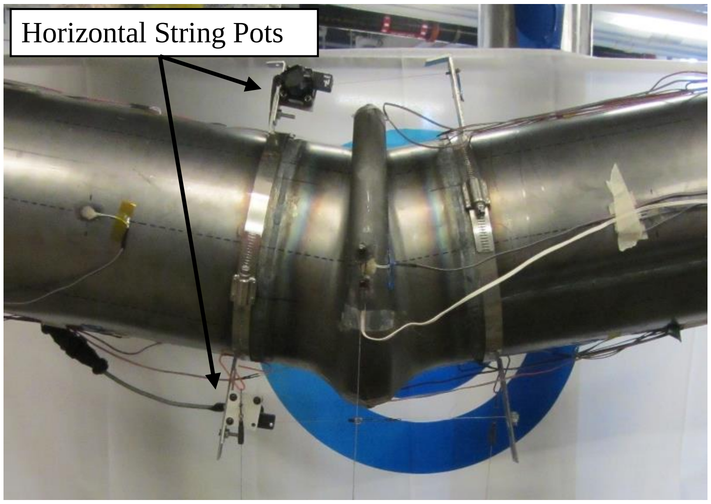

Figure 4.10. Image of Deflected Wave during Four-Point Bending Test Showing Horizontal String Pots

4.4.5. SPF Wave Feature Moment-Rotation

The moment-rotation results for the SPF wave feature are shown in Figure 4.11. The wave rotations are taken as the average of the VSP rotations presented in Figure 4.8. The moment is approximated under the assumptions of idealized beam theory from the load applied by the test frame, P, and distance from support point to loading point, l_s, as

$$M = \frac{P\, l_s}{2} \tag{4.1}$$

where l_s is equal to 48 in. (1.22 m), as shown in Figure 4.1.

The moment-rotation relationship increases at an approximately linear rate until about 5 degrees. The initial rotational stiffness, K_θ, is approximately 550 kip-in./rad (62 kN-m/rad) [9.6 kip-in./deg (1.1 kN-m/deg)]. After 8 degrees the curve flattens until a sharp increase in moment at about 18 degrees. At this rotation the wave feature closed, and metal-to-metal contact at the crown of the wave led to increasing load with additional rotation.

The first test sequence reached a peak moment of 91 kip-in. (10.3 kN-m) at 22.5 deg. At about 27 degrees the specimen was unloaded to reposition the loading table. The unload/reload curve shows that the majority of imposed deformation was plastic, with little elastic rebound. The sharp drop in moment at 33 degrees is a result of an abrupt shift in the north support roller.

The test applied a maximum moment of 94.9 kip-in. (10.7 kN-m) at a maximum rotation of 36.6 degrees, after which loading was discontinued. The decision to stop the experiment was also influenced by the manifestation of longitudinal crimping at the invert of the wave feature, and a desire to understand better this deformation pattern. Photographs of the deformed specimen are presented in the following section.

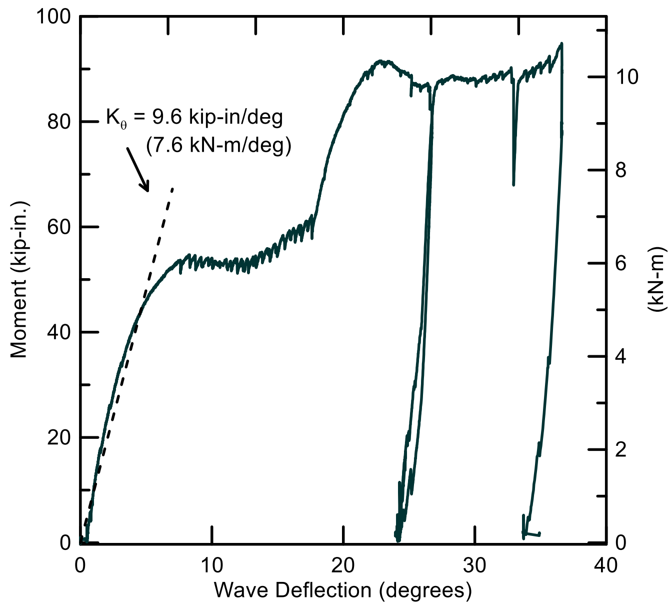

Figure 4.11. SPF Wave Feature Moment-Rotation Response

4.4.6. Deformation of SPF Wave

This section provides images of the test specimen before, during, and following the four-point bending test. Figure 4.12 provides a sequence of photos taken from a video recording of the test. The first three images show the test frame table (bottom of frame) moving upward toward the spreader beam during the test. Figure 4.11(d) shows the second test sequence, after the cross-head and spreader beam had been lowered to provide additional stroke.

(a) Pre-test

(b) Approximately 14 Degrees of Rotation

(c) End of First Loading Stage, 27 Degrees

(d) Maximum Deformation, 36.6 Degrees

Figure 4.12. SPF at Several Levels of Imposed Bending Deformation

4.5. Bending Test Conclusions

A four–point bending test was performed on a 12-ft (4-m)-long section of SS 400 pipe with a JFE wave feature at its midpoint. The pipe was pressurized with water to about 80 psi (550 kPa) throughout the test. Deformation was applied by the test frame in two steps. The initial sequence imposed 11.5 in. (290 mm) of vertical displacement and resulted in a wave deflection of 27 degrees. The specimen was unloaded, and the pipe and loading system was adjusted. The specimen was then reloaded to develop an additional 5.2 in. (132 mm) of vertical displacement that resulted in a maximum wave rotation of 36.6 degrees. The wave feature experienced significant deformation without rupture or loss of internal pressure.

The moment-rotation response of the wave under bending is initially linear. After about 8 degrees the curve flattens until a sharp increase in moment at about 18 degrees. At this rotation level the wave feature closed, and metal-to-metal contact at the crown of the wave led to increasing load with additional rotation.

The first test sequence reached a peak moment of 91 kip-in (10.3 kN-m) at 22.5 deg. The second test sequence reached a maximum moment of 94.9 kip-in (10.7 kN-m) at a maximum rotation of 36.6 degrees. At no point during the test did the pipe rupture or lose pressure.

Section 5
Large Scale Testing of Fault Rupture Effects

5.1. Introduction

This section presents the results of the large-scale fault rupture test performed with a steel pipeline equipped with SPF wave features. All testing was performed in the large-scale test basin at the Cornell University Large Scale Lifelines Testing Facility during July 2016.

5.2. Experimental Setup

Figure 5.1 is a plan view of the test layout which shows the fault rupture plane and approximate locations of the four actuators generating basin movement. The pipeline consisted of a 28.9-ft (8.8 m)-long, continuous welded steel pipeline with two SPF wave features positioned at 18 in. (455 mm) on either side of the fault. The intersection angle between the pipe and fault was 50°. The abrupt ground movement during the test was representative of right-lateral strike-slip fault rupture as well as the most severe ground deformation that occurs along the margins of liquefaction-induced lateral spreads and landslides. The objective of the test was to evaluate the pipeline capacity to accommodate fault movement through the simultaneous axial compression and deflection at each of the two wave features.

The pipeline was buried in the Cornell large-scale test basin in partially saturated sand that was compacted to have an average friction angle of 42º, equivalent in strength to that of a medium dense to dense granular backfill. The 8.5-in. (216-mm) outer-diameter pipe was placed on a bed of soil 11.5 in. (292 mm) in depth. The depth of burial to top of pipe was 40 in. (1.02 m) resulting in 60 in. (1.52 m) of total soil depth. During the test, the south part of the basin remained stationary while the north part was displaced to the south and east by large-stroke actuators to cause soil rupture and slip at the interface between the two parts of the test basin.

The test specimen was manufactured as five discrete sections in Japan, shipped to Cornell, and welded together at four locations along its length. Wave features were welded to either side of a 28.7-in. (729 mm)-long straight section of pipe centered on the fault crossing. The opposing sides of the SPF waves were welded to 150-in. (3.8 m)-long sections of straight pipe equipped with end flanges and pressurization caps.

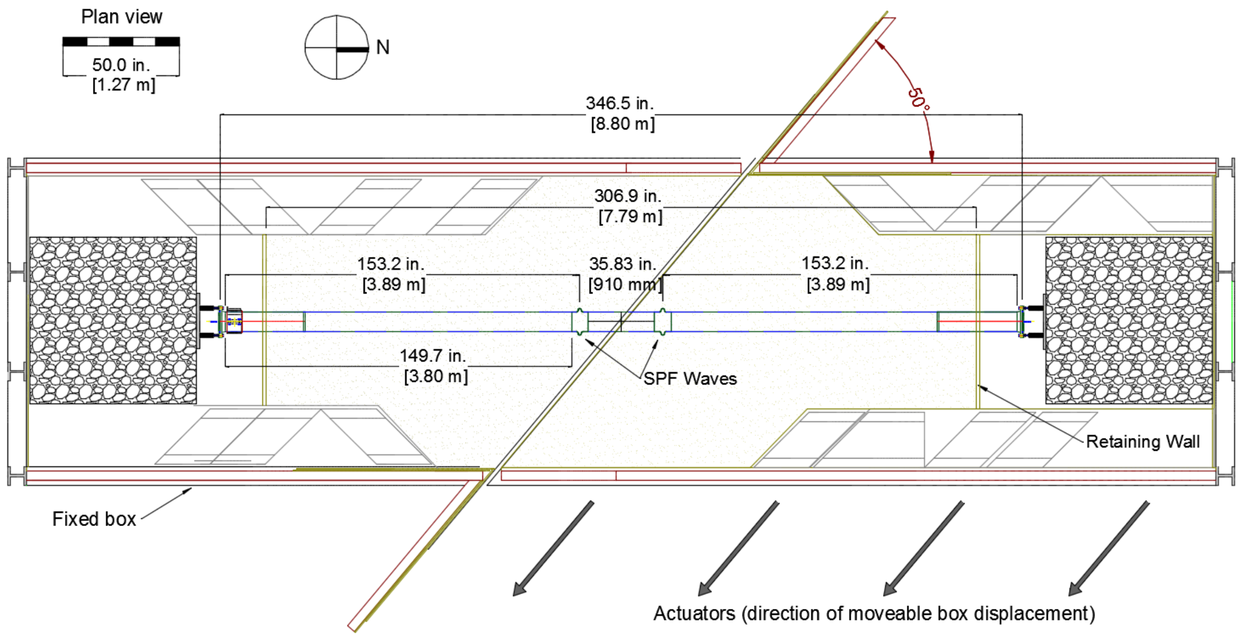

Figure 5.1. Plan View of Pipe Centered SPF Specimen in Test Basin

Figure 5.1 shows that a total length of approximately 25.6 ft (7.8 m) of pipeline was buried in soil. The flanges at each end of the specimen were fixed to the north and south test basins to provide worst-case loading conditions. Parametric finite element analyzes were performed by Cornell to ensure the prescribed length provided burial conditions that would develop the same pipeline response as would occur for a test pipeline length equal to that of the entire test basin. The full length of the test basin was designed to ensure that pipeline bending deformation would not be influenced by the end conditions for pipe diameters as large as 24 in. (0.6 m). Retaining walls were constructed near the ends of the pipeline to allow access to instruments and pressurization fittings. The pipe was pressurized with water to approximately 80 psi (552 kPa). The north (movable) portion of the test basin is connected to four MTS hydraulic actuators with load cells controlled by a MTS Flextest GT controller. All actuators were operated in synchronized displacement control. The test configuration allows the actuators to displace the north half of the test basin a maximum of 48 in. (1.2 m) with a combined force of 326 kips (1450 kN).

5.2.1. Test Procedure

The general test procedure, after all instruments were installed, soil placed, and pipe filled with water, was:

a) Begin data acquisition and start the servo-controlled hydraulic system
b) Introduce and verify internal water pressure
c) Move the test basin 12 in. (300 mm) at a rate of 12 in./minute (300 mm/minute)
d) Verify internal pressure and instrument response
e) Impose a second 12 in. (300 mm) of test basin movement
f) Continue monitoring instruments until 24 in. (600 mm) of total fault displacement

Before beginning the experiment, JFE and Cornell teams discussed an upper bound for fault rupture imposed by split-basin movement. First-order estimates of imposed wave deformation had been made based on the geometry of the test setup and specimen dimensions. These estimates were supplemented by the results of 2D finite element analyses. The intention was to select a maximum fault rupture magnitude that would impose wave deformation that would exceed the suggested design values. Given the fault rupture angle relative to the orientation of the pipeline (50°), the approximate spacing between wave features [36 in. (914 mm)], and the design values for wave axial compression [2 in. (52 mm)] and deflection (18°), various magnitudes of imposed fault rupture were considered. It was decided that a total fault movement of 24 in. (600 mm) could be achieved, thus deforming the pipeline substantially beyond its nominal design values.

5.2.2. Instrumentation

A total of 116 instruments were used to make various measurements during the test. The instrumentation included strain gages at locations (gage planes) along the pipeline, four load cells at each end of the specimen and two digital transducers to measure internal water pressure. Measurements of test basin movement were gathered, including actuator force and displacement and the relative movement between the north and south sections of the test basin.

Figure 5.2 provides the locations of strain gage planes along the test specimen. Ninety-six strain gages were installed at twenty-one planes to measure strains and to evaluate axial forces and bending moments. Strain gages were positioned at the crown (C) and invert (I), and at the east (E) and west (W) springlines of the pipe. All uniaxial and rosette (X-Y pair) gages installed had a gage length of 3 mm.

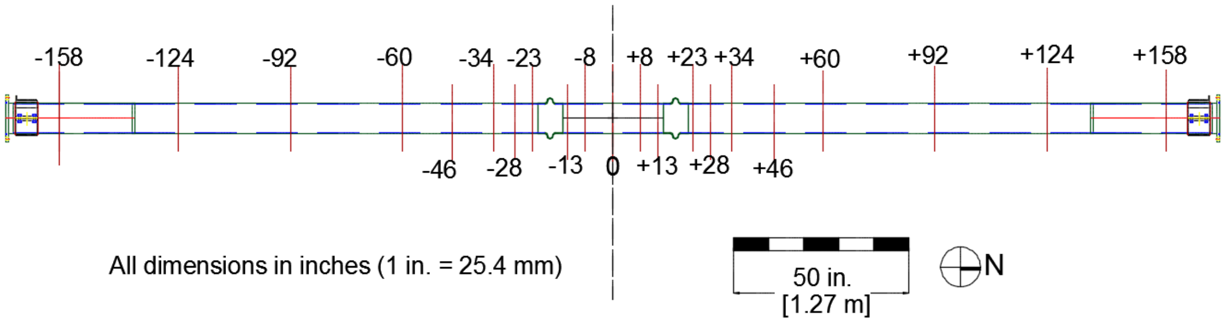

Figure 5.2. Distribution of Strain Gage Planes along SPF Box Test Specimen

Table 5.1 lists the strain gages with respect to distance from the fault and closest wave feature. Each gage number represents the distance (in inches) of the gage from the centerline of the specimen at the fault crossing. Positive (+) designation identifies gages north of the fault while negative (-) gages are positioned on the southern half of the test specimen. Gage planes were positioned symmetrically about the centerline and location of gages at each symmetric plane were mostly identical.

Strain gage plane locations were chosen on the basis of the expected deformed pipeline shape as determined from axial compressive and four-point bending tests previously discussed as well as the results of finite element simulations. Strain gage stations +158 and -158 provide measurements of the end loads. Strain gage stations close to the waves, ±13 and ±23, measured strains concentration near the waves. Four calibrated load cells were positioned at each end of the test basin to measure axial load. Table 5.2 provides the locations and the labeling of the load cells.

Thirty-eight survey marks were scribed along the specimen crown on 12-in. (300-mm) intervals. A denser array of survey marks, on 6-in. (150-mm) intervals, were used within 60 in. (1500 mm) either side of the specimen centerline. The pipe was surveyed with a total station instrument before burial to determine its initial position, and again after the test, to measure pipeline deformation. Typical total station measurement errors were less than 0.25 in. (6 mm). Baseline readings of all measuring devices were taken before pressurizing the pipe, after which temperature variations were minor.

Table 5.1. Strain Gage Locations and Coding System for SPF Split-basin Test

Gage Station	Gages	Distance from Fault	Distance from Closest Wave
±158	±158E - East Springline, Longitudinal ±158C- Crown, Longitudinal ±158W- West Springline, Longitudinal ±158I- Invert, Longitudinal	158 in. (4.01 m)	140 in. (3.56 m)
±124	±124E - East Springline, Longitudinal ±124W- West Springline, Longitudinal	124 in. (3.15 m)	106 in. (2.69 m)
±92	±92E - East Springline, Longitudinal ±92W- West Springline, Longitudinal	92 in. (2.34 m)	74 in. (1.88m)
±60	±60E - East Springline, Longitudinal ±60C- Crown, Longitudinal ±60W- West Springline, Longitudinal ±60I- Invert, Longitudinal	60 in. (1.52 m)	42 in. (1.07 m)
±46	±46E - East Springline, Longitudinal ±46W- West Springline, Longitudinal	46in. (1.17 m)	28 in. (0.71 m)
±34	±34E - East Springline, Longitudinal ±34C- Crown, Longitudinal ±34W- West Springline, Longitudinal ±34I- Invert, Longitudinal	34 in. (0.86 m)	16 in. (0.41 m)
±28	±28E - East Springline, Longitudinal ±28C- Crown, Longitudinal ±28W- West Springline, Longitudinal ±28I- Invert, Longitudinal	28 in. (0.71 m)	10 in. (0.25 m)
-23	-23EA - East Springline, Longitudinal -23CA- Crown, Longitudinal -23WA- West Springline, Longitudinal -23IA- Invert, Longitudinal -23EC - East Springline, Circumferential -23CC- Crown, Circumferential -23WC- West Springline, Circumferential -23IC- Invert, Circumferential	23 in. (0.58 m) south	5 in. (0.13 m) south of south wave
-13	-13EA - East Springline, Longitudinal -13CA- Crown, Longitudinal -13WA- West Springline, Longitudinal -13IA- Invert, Longitudinal -13EC - East Springline, Circumferential -13CC- Crown, Circumferential -13WC- West Springline, Circumferential -13IC- Invert, Circumferential	13 in. (0.33 m) south	5 in. (0.13 m) north of south wave

Table 5.1. Strain Gage Locations and Coding System for SPF Split-basin Test (Completed)

Gage Station	Gages	Distance from Fault	Distance from Closest Wave
-8	-8EA - East Springline, Longitudinal -8CA- Crown, Longitudinal -8WA- West Springline, Longitudinal -8IA- Invert, Longitudinal -8EC - East Springline, Circumferential -8CC- Crown, Circumferential -8WC- West Springline, Circumferential -8IC- Invert, Circumferential	8 in. (0.2 m) south	10 in. (0.25 m) north of south wave
0	0EA - East Springline, Longitudinal 0CA- Crown, Longitudinal 0WA- West Springline, Longitudinal 0IA- Invert, Longitudinal 0EC - East Springline, Circumferential 0CC- Crown, Circumferential 0WC- West Springline, Circumferential 0IC- Invert, Circumferential	0 in. (0 m)	±18 in. (0.46 m) between the two waves
+8	+8EA - East Springline, Longitudinal +8CA- Crown, Longitudinal +8WA- West Springline, Longitudinal +8IA- Invert, Longitudinal +8EC - East Springline, Circumferential +8CC- Crown, Circumferential +8WC- West Springline, Circumferential +8IC- Invert, Circumferential	8 in. (0.2 m) north	10 in. (0.25 m) south of north wave
+13	+13EA - East Springline, Longitudinal +13CA- Crown, Longitudinal +13WA- West Springline, Longitudinal +13IA- Invert, Longitudinal +13EC - East Springline, Circumferential +13CC- Crown, Circumferential +13WC- West Springline, Circumferential +13IC- Invert, Circumferential	13 in. (0.33 m) north	5 in. (0.13 m) south of north wave
+23	+23E – East, Springline, Longitudinal +23C- Crown, Longitudinal +23W- West, Springline, Longitudinal +23I- Invert, Longitudinal	23 in. (0.58 m) north	5 in. (0.13 m) north of north wave

Table 5.2. Load Cell Locations and Labeling for SPF Box Test

Location	Load Cell
South End	SW Top Ld –West, Top SE Top Ld –East, Top SW Bot Ld –West, Bottom SE Bot Ld –East, Bottom
North End	NW Top Ld – West, Top NE Top Ld – Outer, East, Top NW Bot Ld – West, Bottom NE Bot Ld – East, Bottom

5.2.3. Soil Preparation

The soil used during the test was crushed, washed, glacio-fluvial sand obtained from RMS Gravel, Dryden, NY, consisting of particles mostly passing the ¼ in. (6.35 mm) sieve. Figure 5.3 is the grain size distribution of the RMS graded sand. Approximately 8-in. (203-mm)-thick lifts of soil were placed and compacted until there was 40 in. (1.02 m) cover of compacted sand above the pipe crown. Soil placed in close vicinity of the instrumented pipe was compacted with a hand tamper while a vibratory plate compactor was used for soil placed further from the specimen. Every layer was moistened with water in a similar way to achieve uniformity. To ensure consistency throughout the soil mass the extent of compaction and associated moisture content were verified. Dry density measurements were taken for each layer using a Troxler Model 3440 densitometer. Moisture content measurements were obtained using both soil samples and the densitometer at the same locations.

The target value of dry density was γ_{dry} = 106 lb/ft^3 (16.7 kN/m^3), and the target value of moisture content was w = 4.0 %, corresponding to an angle of shearing resistance (friction angle) of the sand of approximately 42º. Six measurements of dry unit weight and moisture content were made for each soil lift. The average and standard deviation of all dry unit weight measurements were 106.5 lb/ft^3 (16.7 kN/m^3) and 1.7 lb/ft^3 (0.26 kN/m^3), respectively. Moisture content measurement had an average of 3.86% and standard deviation of 0.65%. The angle of shearing resistance of the soil, based on correlations with soil unit weight established at Cornell, was 41-42°. The soil strength properties are representative of a well-compacted dense sand.

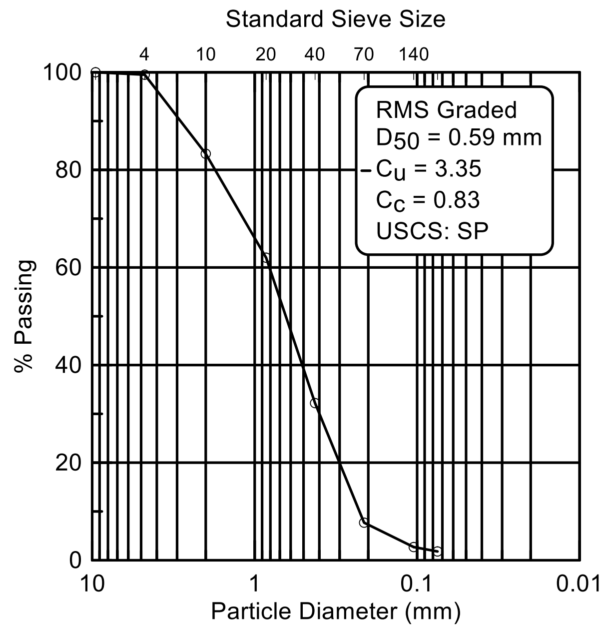

Figure 5.3. Particle Size Distribution of RMS Graded Sand

5.3. Experimental Results of Split Basin Test

Measurements obtained during the fault rupture test are summarized and described under the subheadings that follow.

5.3.1. Test Basin Movements

Four actuators are connected between the movable portion of the test basin and the modular reaction wall in the laboratory. From south to north, the actuators are identified as short-stroke actuator 1 (SSA1), short-stroke actuator 2 (SSA2), long-stroke actuator 1 (LSA1), and long-stroke actuator 2 (LSA2). Each SSA actuator has a displacement range of ± 2 ft (± 0.61 m) for a total stroke of 4 ft (1.22 m) and load capacity of 100 kips (445 kN) tension and 145 kips (645 kN) compression. Each LSA actuator has a displacement range of ± 3 ft (0.91 m) for a total stroke of 6 ft (1.83 m) and load capacity of 63 kips (280 kN) tension and 110 kips (489 kN) compression. The test configuration allows the actuators to displace the north half of the test basin a maximum of 48 in. (1.2 m) with a combined force of 326 kips (1450 kN).

Figure 5.4 shows the displacement of the four actuators, which is equivalent to the fault displacement, with respect to time. Figure 5.5 shows the load vs. time for each actuator. The largest compressive load is required at the actuator closest to the fault. To maintain alignment during the test, a tensile load develops in the northernmost actuator.

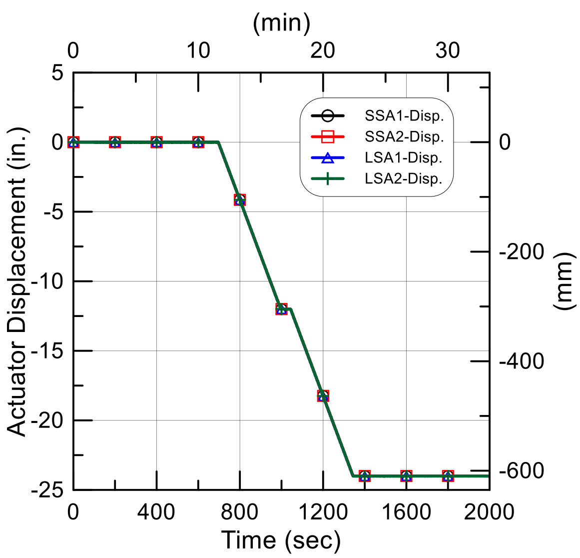

Figure 5.4. Fault Displacement vs. Time

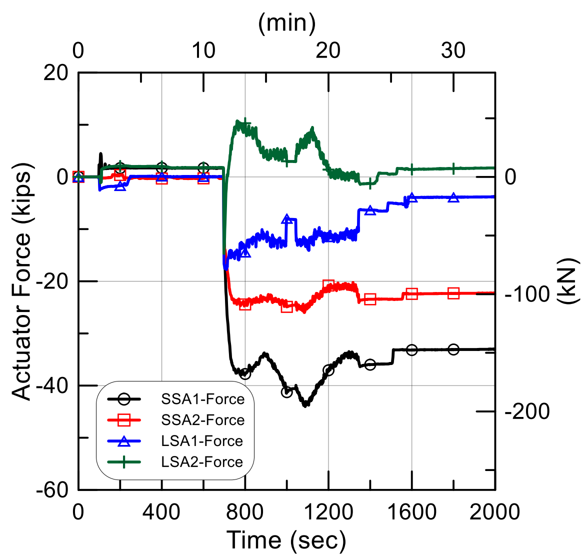

Figure 5.5. Actuator Force vs. Time

5.3.2. Internal Water Pressure

Figure 5.6 shows the pipe internal pressure vs. fault displacement. The pipe was initially pressurized to 80 psi (552 kPa) before basin movement. Movement of the split basin caused the pipeline to decrease slightly in overall length, causing moderate fluctuations in pressure between 80 psi (552 kPa) and 90 psi (621 kPa). Neither rupture nor leakage of the pipeline occurred during the test.

5.3.3. End Loads

The axial compressive loads were measured with four load cells at both the south and north ends of the test basin. The sum of the four load cells at each end of the test basin gives the total axial end load. Figure 5.7 shows the total load at the south and north ends of the test basin vs. fault displacement. Load cell measurements recorded peak force at approximately 13 in. (330 mm) of fault displacement.

Also included in Figure 5.7 are axial loads calculated from axial strain gages at planes close to the end of the test specimen. The axial force from averaged strain gage measurements was calculated as F = εAE, assuming a linear modulus from tensile coupon data, E=31,500 ksi (217 GPa), and constant cross-sectional area, A = 2.4 in^2 (1550 mm^2). Measured axial loads show good agreement throughout the test. Loads recorded at the south end of the specimen were slightly greater than those recorded at the north end.

End loads increased relatively linearly until about 2 in. (50 mm) of fault displacement. The end loads then plateaued until approximately 7 in. (175 mm) when a marked increase in loads developed with further box movement. All load measurements reached a peak value at a fault offset of approximately 14 in. (350 mm), after which they progressively decreased.

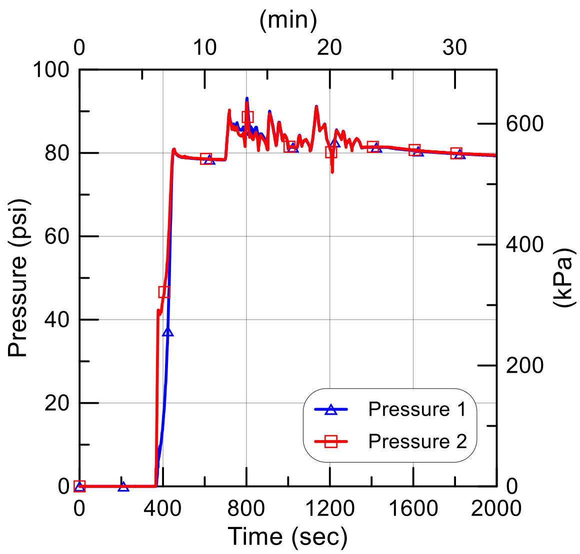

Figure 5.6. Internal Water Pressure vs. Fault Displacement

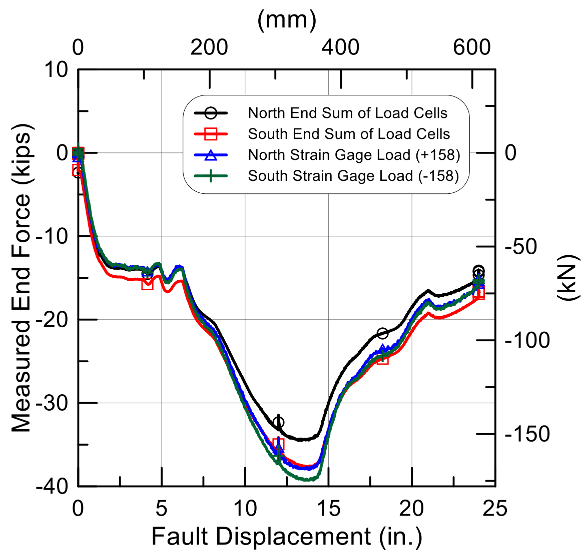

Figure 5.7. Comparison of Average End Force from Load Cells and Strain Gages

5.3.4. Axial Strains

The average axial strains at each gage plane along the pipeline are shown in Figure 5.8 for various levels of fault displacement. The locations of the centers of the wave features at 17.9 in. (455 mm) on either side of the fault are shown in the plots.

Figure 5.8a shows that compressive strains generally increased with increasing fault displacement until 12 in. (300 mm) of fault movement. Relatively constant compressive strains were measured along the pipeline during these initial increments of displacement. Moderate spikes in compressive axial strain are apparent at fault displacements of 8 in. (200 mm) to 12 in. (300 mm) just north of the northern wave feature, indicating a change in stress state in the vicinity of the wave. The increase in average axial compressive strain close to the wave is a product of compressive bending strains adding to the axial compressive strain.

A close examination of Figure 5.8a discloses a relatively large increase in axial compressive strains at both the south and north waves at fault displacements between 6 in. (150 mm) and 8 in. (200 mm). A detailed inspection of the strain gage readings adjacent to the south and north waves shows a sharp change in strain at 6.5 in. (165 mm) of fault movement, which is related to internal contact of the pipe wall in response to compressive deformation of the waves.

Figure 5.8b (note change in scale for strain) shows that, as fault displacement increased from 14 in. (350 mm) to 15 in. (380 mm), axial strains south of the south wave (gage plane -23) became markedly more compressive. The first gage plane south of the north wave (gage plane +13) also registered larger compressive strains as fault movement increased from 16 in. (406 mm) to 17 in. (432 mm).

Figure 5.8c shows that concentrated axial strains were measured at gage planes -23 and +13, located south of the south and north waves, respectively, beyond 17 in. (432 mm) of fault displacement. These gage planes are adjacent to the wave features. As the waves compress and deform, axial buckling propagates into the pipe adjacent to the waves and this buckling is reflected by large average strain values, in excess of 0.3%. The strains are consistent with local plastic deformation associated with axial buckling, as shown by photos of the deformed pipe specimen (Figure 5.11).

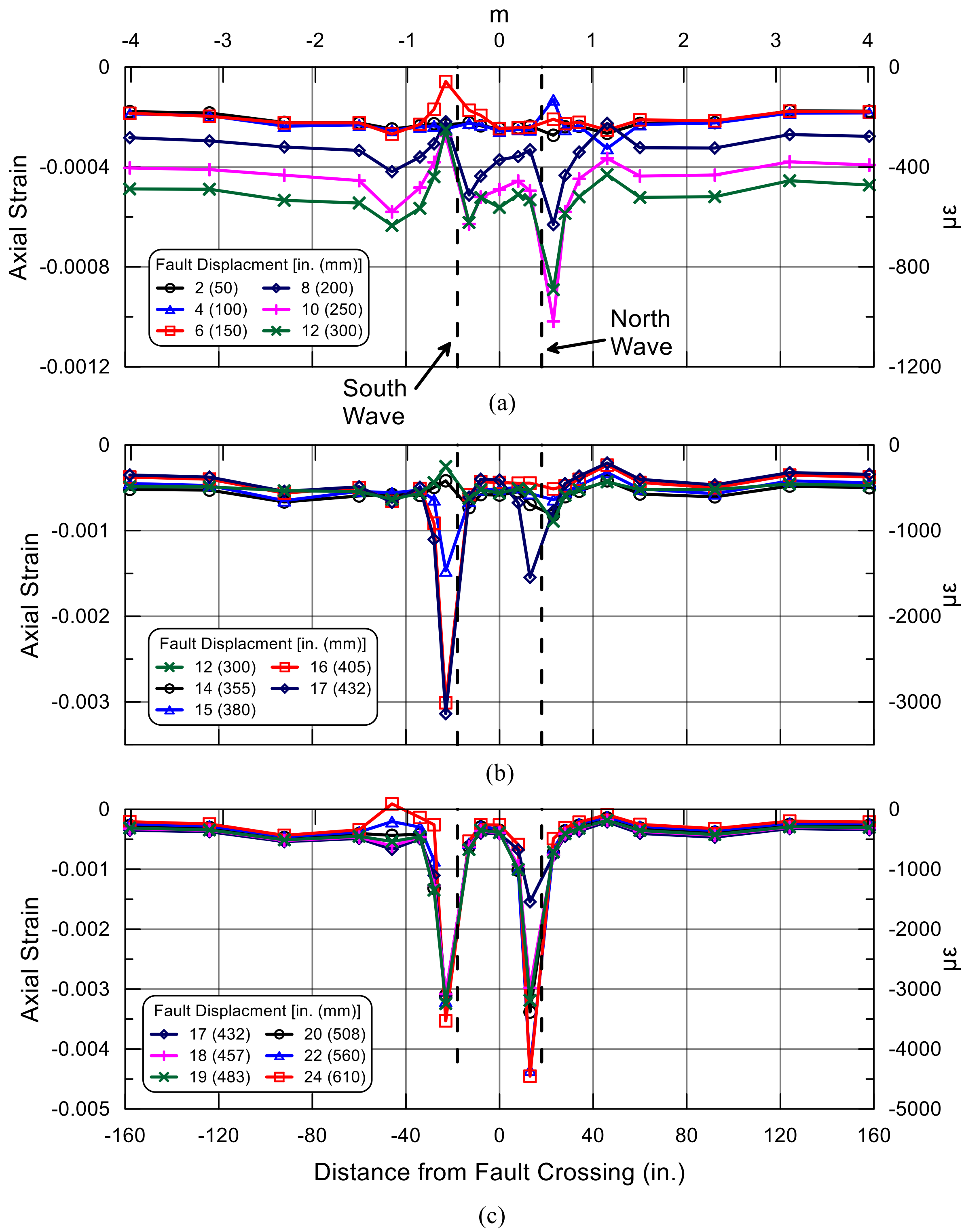

Figure 5.8. Average axial strains along pipeline at (a) 2 to 12 in. (50 to 300 mm), (b) 12 in. to 17 in. (300 to 432 mm), and 17 in. to 24 in. (432 to 610 mm) of fault movement.

5.3.5. Bending Strains

Bending strains were calculated at each strain gage station along the pipe as one half the difference between the springline strains. Figure 5.9 presents the bending strains measured along the pipeline corresponding to various levels of fault displacement. Similar to Figure 5.8, the location of the waves are shown at distances 17.9 in. (455 mm) north and south of the rupture plane.

Figure 5.9a shows that, during the first 12 in. (300 mm) of fault displacement, the bending strains increased as the fault movement increased. The measurements disclose an anti-symmetric pattern of strain distribution centered on the fault.

Figure 5.9b (note change in scale for strain) shows that, as fault displacement reached 15 in. (380 mm), locally high bending strains occurred at gage stations immediately north and south of the north and south wave features, respectively. While bending strains close to the wave features continue to increase at levels of fault displacement greater than 15 in. (380 mm), strains along the pipeline at locations greater than 40 in. (1020 mm) from the fault showed little change, ranging from 0.001 to 0.0014.

Figure 5.9c shows a consistent bending strain distribution for fault movements of 17 in. (430 mm) to 24 in. (610 mm). The maximum bending strain north of the fault shifts from north to south of the north wave feature between 18 in. (457 mm) and 19 in. (483 mm) of fault movement. The maximum bending strains are about 0.003 to 0.004 at 24 in. (610 mm) of fault displacement. The elevated strains are a result of local plastic deformation as axial buckling propagates into the pipe adjacent to the wave features.

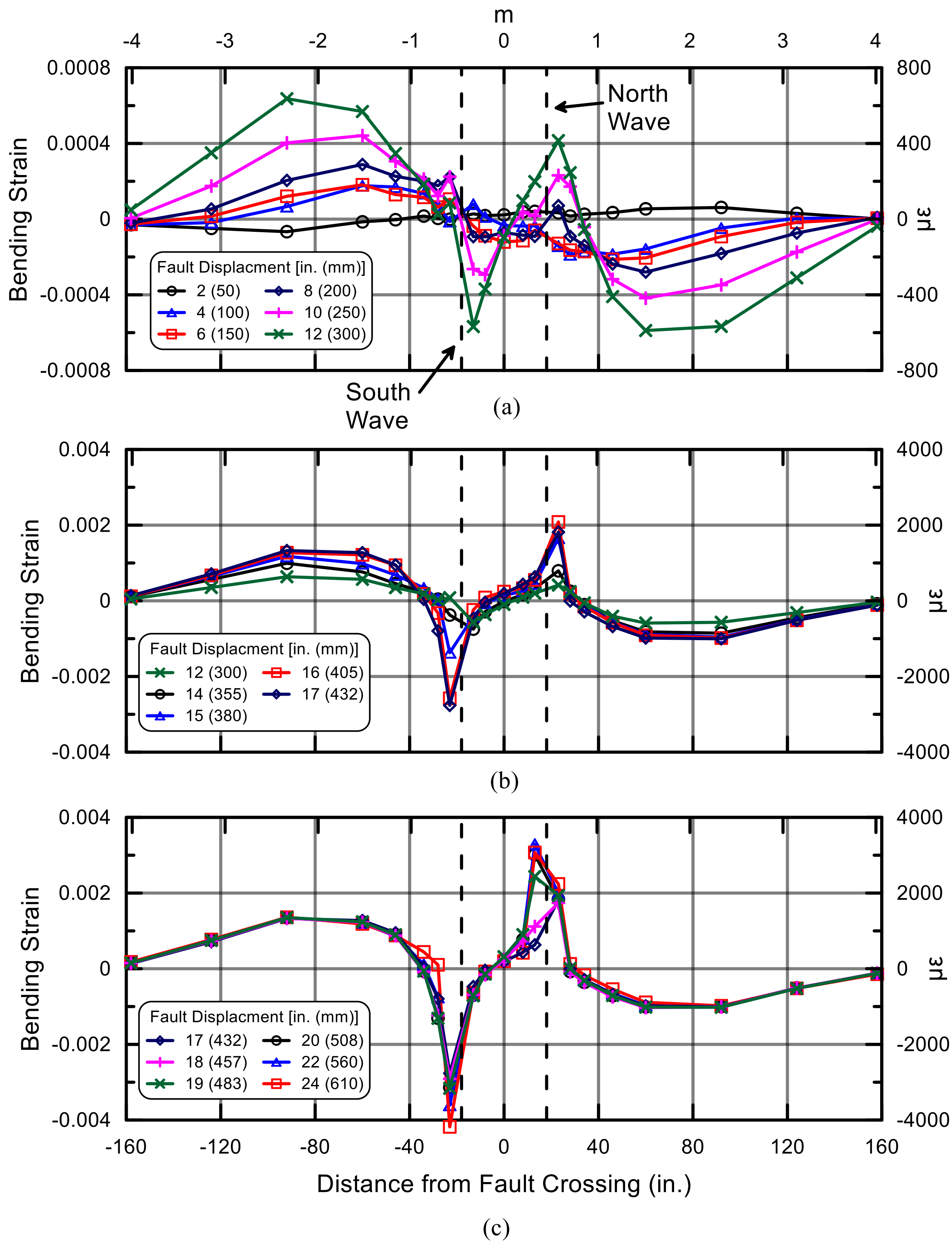

Figure 5.9. Evolution of bending strains along the specimen at (a) 2 to 12 in. (50 to 300 mm), (b) 12 in. to 17 in. (300 to 432 mm), and 17 in. to 24 in. (432 to 610 mm) of fault rupture.

5.3.6. Deformed Shape

The pipeline location was surveyed at thirty-eight points with a total station surveying system before backfilling and burial of the pipe. After fault rupture the pipeline was excavated carefully in a manner that preserved its deformed shape and resurveyed to determine its final position. Figure 5.10 shows the initial and final positions of the specimen. Gaps in the lines show the locations of the wave features. Figure 5.10a shows a plane view of the entire pipeline. As the center section of the pipe between the waves rotated in response to compressive fault offset, the pipeline deformed as illustrated in the figure. Local variations in the deflected shape of the pipe reflect variability in the final total station measurements, which were taken after severe local disturbance of the soil during fault rupture as well as excavation to expose the pipeline.

Figure 5.10b shows an expanded view at the fault with equal scales in each orthogonal horizontal direction. From the surveying points the final pipeline deflections at the south and north waves were 42.3 and 42.4 degrees, respectively. The survey measurements also indicate that at least 3.3 in. (84 mm) of joint closure occurred across each joint. Due to the large imposed displacement, compressive coupling action of the center length of pipe causes some counter-deflection of the north and south lengths of the pipeline.

Figure 5.11 shows photographs of the pipeline in the vicinity of the fault both before and after testing. The photographs are taken from a vertical position above the pipe along the pipeline crown. The composite photograph of the deformed pipe is positioned so that the south wave features before and after the test are at the same location. The deflected shape, axial compression, and lateral offset of the pipe are illustrated in the figure.

5.3.7. Pipe Cross-section

Figures 5.12a and b show photographs of the pipe cross-section in the vicinity of the fault after completion of the test. Figure 5.12a shows the south wave looking north and Figure 5.12b shows the north wave looking south. Even though there is considerable deflection and axial compression at each of the wave features, there is only a limited reduction in cross-sectional area in the central section of the pipeline that crossed the fault. Post-test measurements estimate that the maximum local loss of cross-sectional area was confined to about 18% and 12% of the initial cross-sectional area of the south and north waves, respectfully. Although local flow losses will result from the change in shape of the pipeline at the fault crossing, substantial flow would be able to occur through the cross-sectional area that remains after deformation of the wave features to accommodate fault movement.

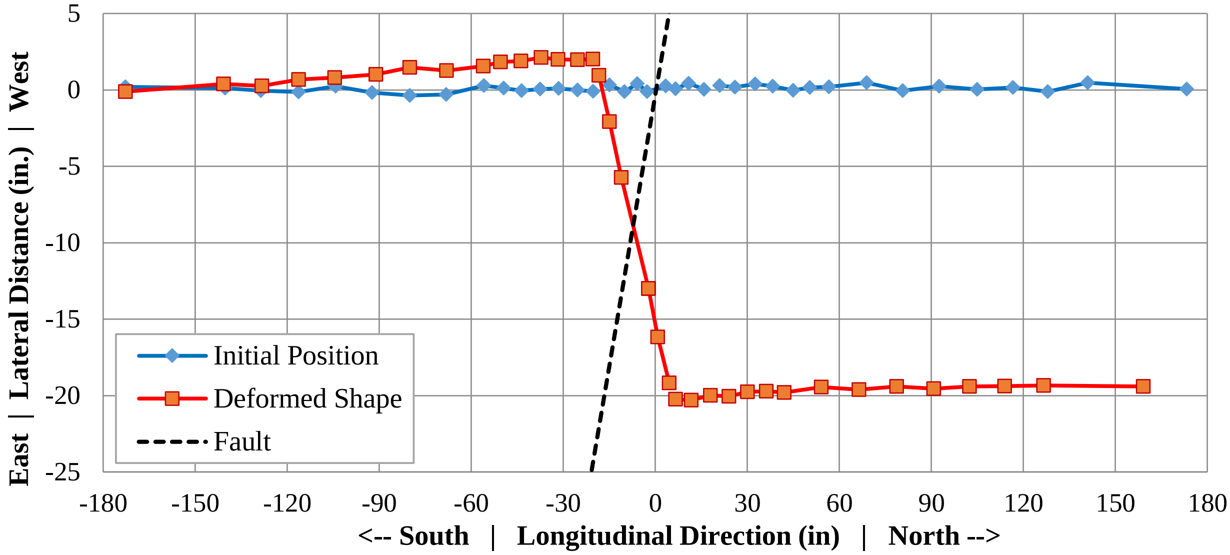

a.) Full pipe length

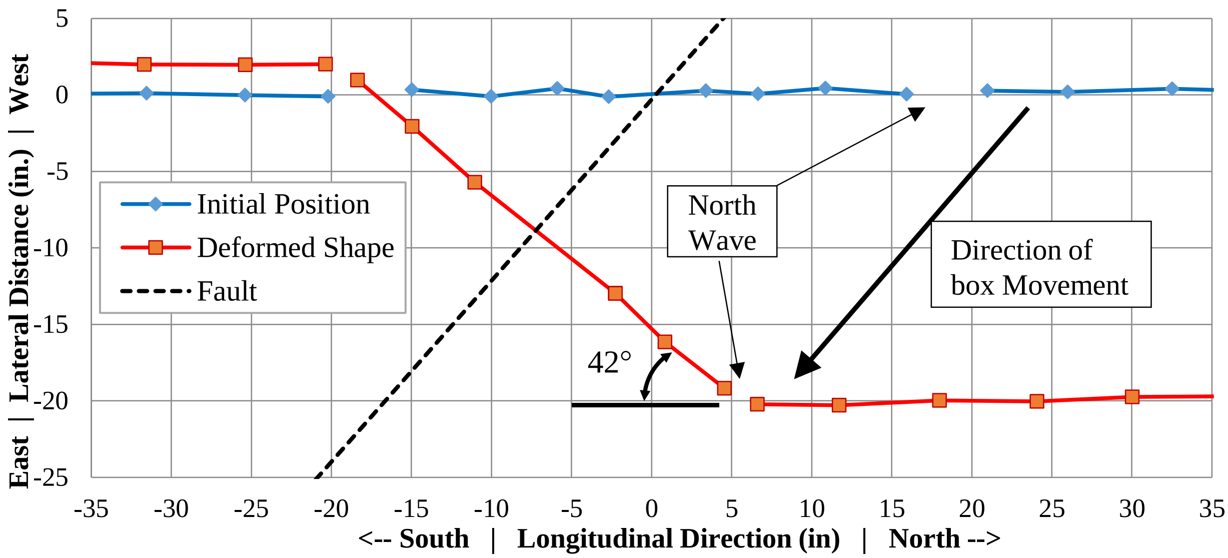

b.) Expanded view at fault (1 in. = 25.4 mm)

Figure 5.10. Initial and Final Position of the Pipe Specimen: (a) Entire Pipe Length with Exaggerated Axis and (b) Center Section of Pipe at Equal Horizontal Scales.

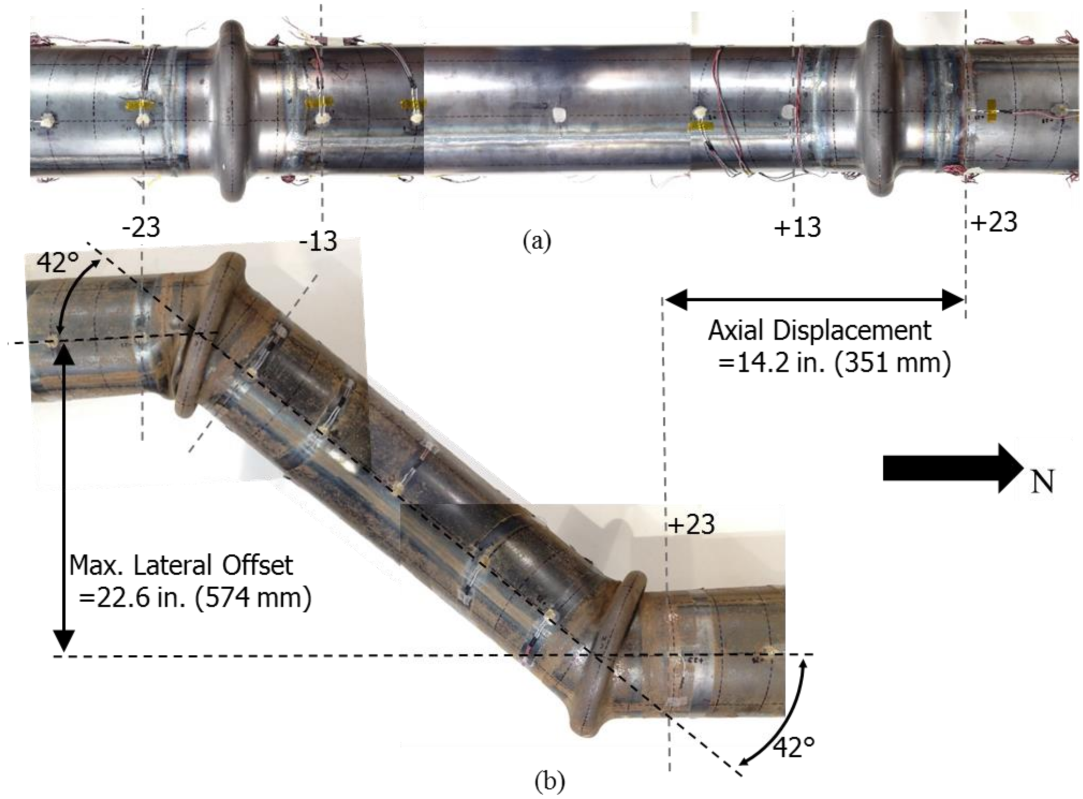

Figure 5.11. Images of Pipeline (a) Before Burial and (b) After Excavation

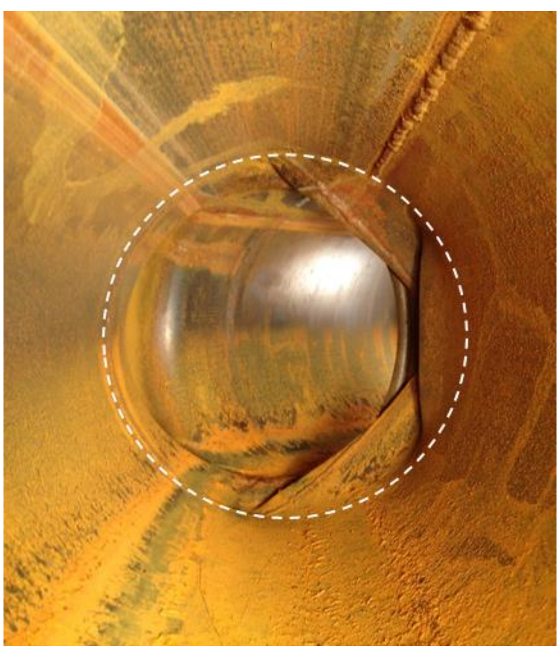

(a) South wave, looking north

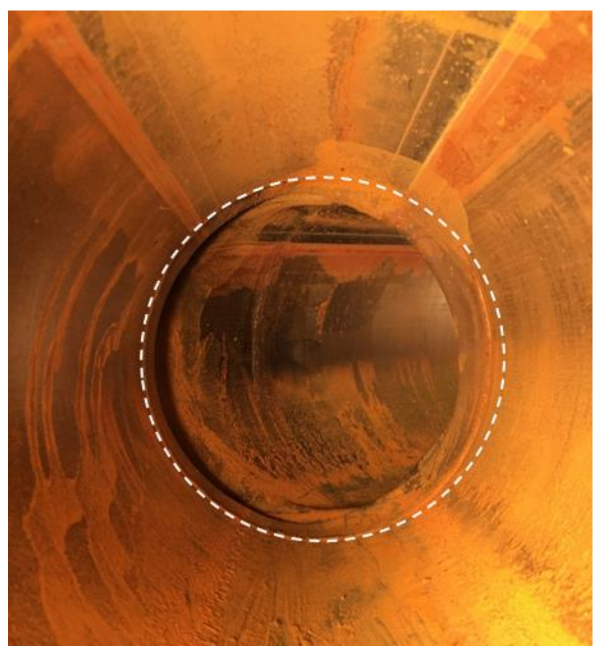

(b) North wave, looking south

Figure 5.12. Photos of Specimen Interior

5.4. Summary of Large-Scale Testing Results

A 28.9-ft (8.8-m)-long, continuous welded steel pipeline with two SPF wave features positioned 18 in. (455 mm) on either side of the fault rupture plane was tested at the Cornell Large-Scale Lifelines Facility. The pipe was instrumented with ninety-six strain gages installed at twenty-one locations along the pipeline to measure strains and to evaluate axial forces and bending moments. Strain gages were positioned at the crown (C), invert (I) east (E) springline, and west (W) springline of the pipe. Four load cells were placed at each end of the specimen, reacting between the test basin structural frame and pipe end restraint to measure axial force. The pipe was pressurized to approximately 80 psi (552 kPa).

The pipeline was buried in the Cornell large-scale test basin in partially saturated sand that was compacted to have an average friction angle of 42º, equivalent in strength to that of a medium dense to dense granular backfill. The depth of burial to top of pipe was 40 in. (1.02 m). During the test, the south part of the basin remained stationary, while the north part was displaced to the south and east by large-stroke actuators to cause soil rupture and slip at the interface between the two parts of the test basin.

The north section of the test basin was displaced along a 50º fault at a rate of 12 in. (300 mm) per minute. The basin was displaced 12 in. (300 mm), followed by brief pause and additional 12 in. (300 mm) of movement along the fault. The 24 in. (600 mm) of total fault movement corresponds to 15.2 in. (392 mm) of axial compression of the basin and pipe. The pipe did not lose pressure or rupture during the test.

The test measurements confirm that the pipeline was able to accommodate substantial fault movement through axial displacement and deflection of the wave features positioned either side of the fault with no pipe rupture or loss of water pressure. Moreover, the measurements provide a comprehensive and detailed understanding of how the movement was accommodated at the waves. The maximum deflection measured across the waves was greater than 42 degrees and the maximum axial compression at each wave was approximately 3.3 in. (84 mm). These results demonstrate the ability of the waves to sustain levels of combined axial compression and deflection that exceed suggested design limits. Moreover, maximum local loss of cross-sectional area was confined to about 12-18% of the initial cross-section of the pipe before fault rupture. Substantial flow would thus be able to occur through the cross-sectional area that remains after deformation of the wave features to accommodate fault movement.

5.4.1. Conclusions

The objective of the test was to impose abrupt ground deformation on the pipeline, which was representative of a right-lateral strike-slip fault rupture and the most severe ground deformation that occurs along the margins of liquefaction-induced lateral spreads and landslides. The pipeline was constructed to evaluate its capacity to accommodate fault movement through the simultaneous axial compression and deflection at each of the two wave features.

The test measurements confirm that the pipeline was able to accommodate fault rupture through axial displacement and deflection of the wave features positioned on either side of the rupture zone. Moreover, the measurements provide a comprehensive and detailed understanding of how the movement was accommodated at the waves, reducing stresses imposed along the straight sections of pipeline. The maximum deflection measured across the waves was greater than 42 degrees and the maximum axial compression at each wave was approximately 3.3 in. (84 mm), thus demonstrating the ability of the waves to sustain significant levels of combined axial compression and deflection.

The JFE SPF wave features were able to accommodate significant fault movement through axial compression and deflection of the waves. Fault rupture simulated in the large-scale test is also representative of the most severe ground deformation that occurs along the margins of liquefaction-induced lateral spreads and landslides.

The amount of compressive strain and deflection that can be accommodated by a steel pipeline with JFE SPF waves will depend on the wave spacing and design. The pipeline used in the large-scale split-basin test was able to accommodate 15.2 in. (392 mm) of axial compression, corresponding to an average compressive strain of 4.4% along the pipeline, without rupture or leakage.

Section 6

Summary

This report presents the test results from a program to investigate the performance of an 8.5-in. (216-mm)-diameter steel pipe with a JFE Wave Feature for Steel Pipe Crossing Faults (SPF). The purpose of the testing is to evaluate the ability of the SPF to accommodate axial and bending deformation and assess how the pipe and its specially shaped wave features respond to fault rupture and other types of abrupt soil movement that may intersect the pipeline. Test results are summarized for SPF compression and bending tests, as well as pipeline response to fault rupture under the headings that follow.

6.1. Tensile Coupon Tests

Uniaxial tension testing was performed on the steel used in JFE pipelines. The test specimens were machined from samples of hot rolled steel plate provided by JFE. Tensile coupons were tested in tension to evaluate the strength, stiffness, and ductility of the material. All testing was conducted in accordance with the ASTM – E8 2013 Standard (ASTM, 2013). The average yield stress, ultimate stress, Young's modulus, and Poisson's ratio determined from the direct tension tests are 44.8 ksi (309 MPa), 65.5 ksi (452 MPa), 31,500 ksi (216 MPa), and 0.29. The results of the tensile coupon tests meet the criteria in the JIS SS400 Standard (JIS G3101, 2015).

6.2. SPF Compression Test

A compression test was performed on a 6.6-ft (2-m)-long section of SS 400 pipe with a wave feature at its midpoint. The pipe was pressurized with water to at least 80 psi (550 kPa) throughout the test. An initial actuator displacement of 3.7 in. (94 mm) was applied, the pipe section and loading system adjusted, and an additional 3 in. (75 mm) displacement applied. The wave feature experienced significant deformation without rupture or reduction of internal pressure.

At a wave displacement of 0.21 in. (5.3 mm) the pipe reached a peak force of 17.9 kip (79.6 kN), after which the force decreased until a wave displacement of roughly 1.86 in. (47.2 mm). At this point the wave feature closed and the pipe compressive force increased. At no point during the test did the pipe rupture or lose pressure. The test was continued until a wave displacement of approximately 6 in. (152 mm) without loss of pressure.

6.3. SPF Bending Test

A four–point bending test was performed on a 12-ft (4-m)-long section of SS 400 pipe with a wave feature at its midpoint. The pipe was pressurized with water to about 80 psi (550 kPa) throughout the test. Deformation was applied by the test frame in two steps. The initial sequence imposed 11.5 in. (290 mm) of vertical displacement and resulted in a wave deflection of 27 degrees. The specimen was unloaded, and the pipe and loading system was adjusted. The specimen was then reloaded to develop an additional 5.2 in. (132 mm) of vertical displacement that resulted in a maximum wave rotation of 36.6 degrees. The wave feature experienced significant deformation without rupture or loss of internal pressure.

The moment-rotation response of the wave under bending is initially linear. After about 8 degrees the curve flattens until a sharp increase in moment at about 18 degrees. At this rotation level the wave feature closed, and metal-to-metal contact at the crown of the wave led to increasing load with additional rotation.

The first test sequence reached a peak moment of 91 kip-in (10.3 kN-m) at 22.5 deg. The second test sequence reached a maximum moment of 94.9 kip-in (10.7 kN-m) at a maximum rotation of 36.6 degrees. At no point during the test did the pipe rupture or lose pressure.

6.4. Large Scale Testing of Fault Rupture Effects

A 28.9-ft (8.8-m)-long, continuous welded steel pipeline with two SPF wave features positioned 18 in. (455 mm) on either side of the fault rupture plane was tested at the Cornell Large-Scale Lifelines Facility. The pipe was instrumented with ninety-six strain gages installed at twenty-one locations along the pipeline to measure strains and to evaluate axial forces and bending moments. Strain gages were positioned at the crown (C), invert (I), east (E) springline, and west (W) springline of the pipe. Four load cells were placed at each end of the specimen, reacting between the test basin structural frame and pipe end restraint to measure axial force. The pipe was pressurized to approximately 80 psi (552 kPa).

The pipeline was buried in the Cornell large-scale test basin in partially saturated sand that was compacted to have an average friction angle of 42º, equivalent in strength to that of a medium dense to dense granular backfill. The depth of burial to top of pipe was 40 in. (1.02 m). During the test, the south part of the basin remained stationary, while the north part was displaced to the south and east by large-stroke actuators to cause soil rupture and slip at the interface between the two parts of the test basin.

The north section of the test basin was displaced along a 50º fault at a rate of 12 in. (300 mm) per minute. The basin was displaced 12 in. (300 mm), followed by brief pause and additional 12 in. (300 mm) of movement along the fault. The 24 in. (600 mm) of total fault movement corresponds to 15.2 in. (392 mm) of axial compression of the basin and pipe. The pipe did not lose pressure or rupture during the test.

The test measurements confirm that the pipeline was able to accommodate substantial fault movement through axial displacement and deflection of the wave features positioned either side of the fault with no pipe rupture or loss of water pressure. Moreover, the measurements provide a comprehensive and detailed understanding of how the movement was accommodated at the waves. The maximum deflection measured across the waves was greater than 42 degrees and the maximum axial compression at each wave was approximately 3.3 in. (84 mm), thus demonstrating the ability of the waves to sustain significant levels of combined axial compression and deflection. Moreover, maximum local loss of cross-sectional area was confined to about 12-18% of the initial cross-section of the pipe before fault rupture, thus substantial flow would be able to occur through the cross-sectional area that remains after deformation of the wave features to accommodate fault movement.

6.5. Significance of Test Results

Large-scale fault rupture tests at Cornell demonstrate the ability of the JFE SPF wave features to accommodate significant fault movement through axial compression and deflection of the waves. Fault rupture simulated in the large-scale test is also representative of the most severe ground deformation that occurs along the margins of liquefaction-induced lateral spreads and landslides.

Direct scaling of the test results to nominal pipeline diameters in the range of 32 in. (~0.8 m) or more imply that JFE SPF pipelines have the ability to accommodate fault displacements on the order of 8 ft. (2.4 m) or more without pipe rupture or significant loss of water pressure for fault crossing angles similar to that tested at Cornell. This estimate assumes that water pressure is sustained in the pipe to reduce the potential for ovaling and cross-sectional buckling of pipe with a diameter-to-wall thickness ratio similar to that tested at Cornell.

The amount of compressive strain that can be accommodated with JFE SPF pipelines will depend on the number and spacing of wave features relative to the location of abrupt ground movement. The pipeline used in the large-scale split-basin test was able to accommodate 15.4 in. (392 mm) of axial compression, corresponding to an average compressive strain of 4.4% along the pipeline. Such compression is large enough to accommodate the great majority (over 99%) of liquefaction-induced compressive ground strains measured by high resolution LiDAR after each of four major earthquakes during the recent Canterbury Earthquake Sequence (CES) in Christchurch, NZ (Bouziou, et al., 2015; O'Rourke, et al., 2014). To put the CES ground strains in perspective, liquefaction-induced ground deformation measured in Christchurch exceed those documented in San Francisco during the 1989 Loma Prieta earthquake (e.g., O'Rourke and Pease, 1997; Pease and O'Rourke, 1997) and in the San Fernando Valley during the 1994 Northridge earthquake (e.g., O'Rourke, 1998). They are comparable to the levels of most severe liquefaction-induced ground deformation documented for the 1906 San Francisco earthquake, which caused extensive damage to the San Francisco water distribution system (e.g., O'Rourke and Pease, 1997; O'Rourke, et al., 2006).

Based on the results of the testing program reported herein, the JFE-SPF system performs well under large-scale compressive loading. Moreover, the tensile coupon and large-scale test results indicate that the JFE SPF system will likely perform well under large-scale tensile loading. It is recommended that large-scale testing be performed to quantify and confirm tensile performance of the JFE SPF system.

Acknowledgements

The authors wish to recognize the excellent effort of Cornell graduate and undergraduate students that made these experiments successful. Namely, the contributions of Christina Argyrou, Chalermpat (Pat) Pariya-Ekkasut, Addie Lederman, Blake Burger, Andrew Shakalis, Margaret Slack, Charles Sanderson, and David Hutter are gratefully acknowledged. Welding expertise was provided by Mike Palmer of the Cornell Synchrotron.

References

ASTM International (2013). "Standard Test Methods for Tension Testing of Metallic Materials", *ASTM Standards*. E8/E8M - 13a, 1 – 28.

Bouziou, D., T.D. O'Rourke, M. Cubrinovski, and D. Henderson (2015) "Evaluation of Ground Deformations during the 2010-2011 Canterbury Earthquake Sequence", Proceedings, 6th Intl. Conf. on Earthquake Geotech. Engr., Christchurch, NZ, 8.

Hasegawa, N. (2013) "Seismic Design Approach for Steel Pipelines Crossing Active Faults", Proceedings, 13th East Asia-Pacific Conference on Structural Engineering and Construction, Sapporo, Japan.

Japanese Standards Association, "Rolled Steel for General Structure," JIS G 3010, 2015 Ed., Aug. 2015.

O'Rourke, T.D. (1998). "An Overview of Geotechnical and Lifeline Earthquake Engineering", Geotechnical Special Publication No. 75, ASCE, Reston, VA, Proceedings of Geotechnical Earthquake Engineering and Soil Dynamics Conference, Seattle, WA, Aug. 1998, Vol. 2, pp.1392-1426.

O'Rourke, T.D. and J.W. Pease (1997). "Mapping Liquefiable Layer Thickness for Seismic Hazard Assessment", Journal of Geotechnical Engineering, ASCE, New York, NY, Vol. 123, No.1, January, pp. 46-56.

O'Rourke, T.D., A. Bonneau, J. Pease, P. Shi, and Y. Wang (2006). "Liquefaction Ground Failures in San Francisco", Earthquake Spectra, EERI, Oakland, CA, Special 1906 San Francisco Earthquake, Vol. 22, No. 52, Apr., pp. 691-6112.

O'Rourke, T.D., Jeon, S-S., Toprak, S., Cubrinovski, M., Hughes, M., van Ballegooy, S., and Bouziou, D. (2014) "Earthquake Response of Underground Pipeline Networks in Christchurch, NZ", Earthquake Spectra, EERI, Vol. 30, No.1, pp. 183-204.

Pease, J.W. and T.D. O'Rourke (1997), "Seismic Response of Liquefaction Sites", Journal of Geotechnical Engineering, ASCE, New York, NY, Vol. 123, No. 1, January, pp. 37-45.